NASA TECHNICAL MEMORANDUM

NASA TM X-3292

NASA TM X-3292

MEASUREMENTS OF FARFIELD SOUND GENERATION FROM A FLOW-EXCITED CAVITY

Patricia J. W. Block and Hanno Heller

Langley Research Center
Hampton, Va. 23665

NATIONAL AERONAUTICS AND SPACE ADMINISTRATION • WASHINGTON, D. C. • DECEMBER 1975

1. Report No.	2. Government Accession No.	3. Recipient's Catalog No.
NASA TM X-3292		

4. Title and Subtitle	5. Report Date
MEASUREMENTS OF FARFIELD SOUND GENERATION FROM A FLOW-EXCITED CAVITY	December 1975
	6. Performing Organization Code
7. Author(s)	8. Performing Organization Report No.
Patricia J. W. Block and Hanno Heller	L-10376
	10. Work Unit No.
9. Performing Organization Name and Address	505-03-12-03
NASA Langley Research Center Hampton, Va. 23665	11. Contract or Grant No.
	13. Type of Report and Period Covered
12. Sponsoring Agency Name and Address	Technical Memorandum
National Aeronautics and Space Administration Washington, D.C. 20546	14. Sponsoring Agency Code

15. Supplementary Notes

Hanno Heller: Bolt Beranek and Newman, Inc., Boston, Massachusetts.

16. Abstract

Results of 1/3-octave-band spectral measurements of internal pressures and the external acoustic field of a tangentially blown rectangular cavity are compared. Proposed mechanisms for sound generation are reviewed. Spectra and directivity plots of cavity noise are presented. Directivity plots show a slightly modified monopole pattern. Frequencies of cavity response are calculated using existing predictions and are compared with those obtained experimentally. The effect of modifying the upstream boundary layer on the noise is investigated and its effectiveness was found to be a function of cavity geometry and flow velocity.

17. Key Words (Suggested by Author(s))	18. Distribution Statement
Cavity noise Aerodynamic sound Directivity	Unclassified - Unlimited Subject Category 71

19. Security Classif. (of this report)	20. Security Classif. (of this page)	21. No. of Pages	22. Price*
Unclassified	Unclassified	45	$3.75

*For sale by the National Technical Information Service, Springfield, Virginia 22161

MEASUREMENTS OF FARFIELD SOUND GENERATION FROM A FLOW-EXCITED CAVITY

Patricia J. W. Block and Hanno Heller*
Langley Research Center

SUMMARY

Results of 1/3-octave-band spectral measurements of internal pressures and the external acoustic field of a tangentially blown rectangular cavity are compared. Proposed mechanisms for sound generation are reviewed. Spectra and directivity plots of cavity noise are presented. Directivity plots show a slightly modified monopole pattern. Frequencies of cavity response are calculated using existing predictions and are compared with those obtained experimentally. The effect of modifying the upstream boundary layer on the noise is investigated and its effectiveness was found to be a function of cavity geometry and flow velocity.

INTRODUCTION

Airframe noise, which is the noise produced by airflow over an aircraft, has been recently recognized as the noise floor for aircraft noise reduction (refs. 1 and 2). Subsequently, much research effort has been aimed at identifying the noise sources on the airframe and determining their relative contribution to the overall airframe aerodynamic noise.

In 1974, Healy (ref. 3) presented a technique for estimating the level of the overall airframe noise and a nondimensionalized airframe-noise spectrum for an aircraft in the cruise configuration. Gibson (ref. 4) extended the applicability of this technique to larger aircraft in the cruise configuration and further investigated the noise produced by the individual components present in the landing configuration such as the main and front wheel wells, landing gear, and flaps. He reports a substantial increase in perceived noise level when the aircraft changes from the cruise to the landing configuration and concludes that the main contributors to the noise increase were the landing-gear/wheel-well assembly and the wing/flap assembly.

A state-of-the-art review of airframe noise by Hardin (ref. 5) revealed a number of papers concerning the production of sound by many types of aerodynamic surfaces in a flow including cavities. A rectangular cavity is the simplest model which can be used to describe the wheel well on an airframe. However, the majority of the papers concerning cavities were

---

*Bolt Beranek and Newman, Inc., Boston, Massachusetts.

aimed only at understanding or reducing the large-scale internal cavity pressure oscillations that occur in such an arrangement. The magnitude of this internal pressure field was found to be a function of fluid velocity, cavity dimensions, and the type of boundary layer preceeding the cavity and the spectrum was shown to take on a periodic or random character depending on these same parameters. Although sound radiation was observed there was no comparison of the internal pressure field with the external sound field nor directivity measurements in these studies, in fact no quantitative measurement of the external sound field was made.

It appears reasonable to assume that the internal pressure field, which has been measured extensively (refs. 6 to 17), is related to the external sound field (ref. 8). If this relationship is strong, the sound-producing mechanisms can be understood in terms of the models already put forth in these references as the cause of the large pressure fluctuations inside the cavity. Further, the application of internal pressure reducing designs could apply to noise reduction.

The intent of this paper is to investigate the effect of the change in velocity, cavity length, and boundary-layer thickness on the farfield sound generated by a flow-excited cavity. Predictions schemes will be reviewed and presented in light of the data obtained in this experiment. The present work contains preliminary sound-field measurements at eight farfield positions with respect to a simple rectangular cavity blown tangentially by a jet. It reports the first systematic attempt to measure the amplitude, spectra, and directivity of farfield radiated cavity noise. The external sound field is compared with internal pressure field which was measured at one point within the cavity.

SYMBOLS

c	speed of sound
D	cavity depth, cm
f	frequency, Hz
f_m	modal frequency, Hz, where $m = 1, 2, \ldots$
k_v	ratio of average vortex convection velocity to the free-stream velocity
L	streamwise length of the cavity, cm
M	Mach number
m	mode number

p	acoustic pressure inside cavity, N/m^2 (Pa)
p_o	peak pressure at open end of cavity, N/m^2 (Pa)
$\mathcal{R}$	acoustic radiation resistance
U	convection velocity in the shear layer over the cavity, m/sec
V	free-stream velocity, m/sec
W	cavity width (span), cm
$\mathcal{X}$	acoustic radiation reactance
X,Y,Z	Cartesian coordinate axes
θ	polar angle, deg
ϕ	azimuthal angle, deg

Subscripts:

L	length
W	width

EXPERIMENTAL ARRANGEMENT AND INSTRUMENTATION

Detailed description of the anechoic facility used in this experiment may be found in reference 18. The experimental arrangement is shown in figure 1. The numbers on the figures correspond to the location of the pressure sensors. Table I lists the angular location of each sensor where θ and ϕ are the polar and azimuthal angles, respectively. The airflow was provided through a 7.6-cm-square nozzle mounted to a flat plate in which the cavity was placed. The plate was long enough so that the trailing-edge noise from the plate was not appreciable. Test velocities were 43 and 86 m/sec. The cavity was placed approximately 2.5 cm from the edge of the square nozzle. The trailing edge of the cavity (see fig. 1(b)) was at least 15 cm upstream of the expected transition region of the jet for all configurations. The cavity configurations that were tested are listed in table II. The entire sequence of tests was repeated with a roughness element located on the lower lip of the

nozzle as shown in figure 1(a). Eight farfield microphones (sensors 2 to 9) shown in figure 1 were placed approximately 0.8 m from the leading edge of the cavity to measure radiated sound produced by the flow-excited cavity. This distance placed the microphones in the far-field geometrically and acoustically for frequencies above about 900 Hz. Sensors 2, 6, 7, and 9 were located beyond the edge of the flat plate but in the same plane. Sensor 1 was located in the center of the rearward facing wall of the cavity to measure the dynamic pressure at this point inside the cavity.

The instrumentation used to obtain the data consisted of nine pressure sensors and their power supplies, amplifiers for signal conditioning, a real-time 1/3-octave analyzer, and an x-y plotter. Sensor 1 was a 1/4-inch piezoelectric dynamic pressure sensor with flat frequency response from 10 Hz to 20 kHz and a linear amplitude response (1 percent) to 180 dB $\left(\text{re } 2 \times 10^{-5} \text{ N/m}^2\right)$. Sensors 2 to 9 were 1/2-inch free-field condenser microphones with flat frequency response to 40 kHz. For each test condition (table II) on-line data were obtained for each sensor in the form of 1/3-octave-band spectra. All pressure levels (hydrodynamic and acoustic) are relative to 2×10^{-5} N/m^2.

BACKGROUND

In order to understand better the data obtained in this experiment it is beneficial to review the mechanisms that have been proposed as the cause of both the random and the large-scale pressure fluctuations inside the cavity. There are four basic types of mechanisms or flow patterns. These source mechanisms can be classified as primary hydrodynamic or primary acoustic. These mechanisms can be described with the help of figure 2 where the cavity is viewed from the side and the flow is moving from left to right. The first source type, which is purely hydrodynamic, is called the captive-vortex model and is shown in figure 2(a). Captive vortices (cellular flow) have been observed for certain values of the cavity length-to-depth ratio (refs. 8 and 12). The oscillatory motion of this captive-vortex system within the cavity has been considered as a cause of large-scale periodic pressure fluctuations (refs. 7, 8, and 12). When the cavity dimensions did not permit cellular flow, the large-scale steady pressure oscillations diminished and the internal pressures were random. These flow patterns were observed in deeper cavities where the length-to-depth ratio was less than about 2.

The second type of source mechanism arises from the shear-layer oscillation which is shown in figure 2(b). Shear-layer oscillation (similar to that occurring with edge tones and vortex formation) is caused by the interaction of the shear layer shed by the leading edge of the cavity with the downstream edge of the cavity. This shear layer is folded into the cavity to form a vortex. As the vortex grows and travels down the cavity length the shear layer moves upward. As the vortex exits from the cavity as a whole, it causes the shear layer to bend into the cavity. After the vortex is shed, the downward position of the shear layer

caused by the mass exit forces the fluid to enter the cavity. At this point another vortex begins to form. Smoke tunnel photographs (ref. 9) and shadowgraphs (ref. 13) show this flow sequence clearly. The explanation and analysis originally given by Nyborg (ref. 6) for this jet/edge interaction was extended by Spee (ref. 14) for a cavity, obtaining a relationship for the frequencies of this type of shear-layer oscillation:

$$\tan \frac{2\pi f_m L}{U} = \frac{2\pi f_m L}{U} \qquad (m = 1, 2, \ldots) \qquad (1)$$

The normal displacement of the shear layer over the mouth of the cavity is similar to the mechanism that excites a Helmholtz resonator. The resonance of the volume of air within the cavity is also thought to enhance the sound radiation for deep cavities when excited in this manner in the resonance region of the cavity (ref. 9).

Another mechanism causing shear-layer oscillation is that proposed by Heller and Bliss (ref. 17) as the result of pressure measurements and a water-table visualization study. Consider a shallow cavity under an external high-speed flow. It appears that at the cavity trailing edge there occurs a periodic mass intake and mass efflux, caused by an oscillatory motion of the shear layer at the trailing edge. The mass intake creates a region of overpressure in the trailing-edge region which sends out an internal pressure front, traveling upstream within the cavity towards the leading edge. There it reflects and travels downstream back towards the trailing edge. This cavity internal pressure wave forces the shear layer "up," since the pressure-wave front divides a region of overpressure and underpressure, to which the shear layer necessarily has to adjust. Hence, the shear layer will bulge out into the free stream when above a region of overpressure and cave in when above a region of underpressure. Thus, the shear layer will assume some wavelike motion which is a result of the cavity internal pressure-wave motion, leading to a periodic up-and-down motion at the trailing edge, which in turn creates the overpressure necessary to sustain the process. Obviously there is a self-sustaining feedback mechanism involved. At subsonic flow speeds, which are of interest in the context of this paper, the shear layer will tend to roll up, forming discrete vortices. Hence, the appearance of discrete vortices is considered in this study as a byproduct of the shear-layer motion. The frequencies of this type motion are given by equation (2).

The third mechanism is a hydrodynamic/acoustic feedback model suggested by Rossiter (ref. 13) and shown in figure 2(c). An interaction of the intense sound emanating from the trailing edge with the shear layer will maintain a periodic shedding of vortices at the leading edge. As these vortices travel downstream and impinge on or pass the trailing edge sound is emitted. This sound travels upstream to interact with the shear layer at the leading edge, and the process is repeated. Rossiter obtained the following empirical prediction formula for the frequency of the periodic pressure fluctuations:

$$f_m = \frac{V}{L} \frac{m - 0.25}{\frac{1}{k_v} + M} \qquad (m = 1, 2, \ldots) \qquad (2)$$

In reference 16, Heller, Holmes, and Covert modified Rossiter's formula in order to improve the frequency prediction for higher Mach numbers. However, they point out that for Mach numbers below 0.5 his formula underpredicts the resonant frequency.

The above three models are examples of hydrodynamic resonance. The captive vortex model is dependent on all dimensions whereas the oscillating-shear-layer and feedback models have preferred frequency predictions based on length only. All three models have velocity dependence. It is conceivable that under the proper conditions (dimensions and velocity) any, all, or none of the mechanisms for oscillatory response may exist.

The fourth type of source mechanism, which is purely acoustic, is called an acoustic resonator and is shown in figure 2(d). Broadband sound generated in the shear layer excites the acoustic modes of the cavity. This model may have length, depth, and width modes. The frequency of the axial-width and axial-length standing wave modes are easily calculated from the formulas

$$f_{mW} = \frac{mc}{2W} \quad \text{and} \quad f_{mL} = \frac{mc}{2L} \qquad (m = 1, 2, \ldots) \qquad (3)$$

respectively. To calculate the frequencies of the depth modes however an expression for the acoustic impedance of the open face is necessary. This approach was taken by Plumblee, Gibson, and Lassiter (ref. 11) who treated the cavity as an acoustic enclosure with five hard surfaces and one finite impedance surface. The expression obtained for a depth mode pressure response is:

$$\frac{p}{p_o} = \left[\left(\mathcal{R}(M,W,L) \sin \frac{2\pi f D}{c} \right)^2 + \left(\mathcal{X}(M,W,L) \sin \frac{2\pi f D}{c} - \cos \frac{2\pi f D}{c} \right)^2 \right]^{1/2} \qquad (4)$$

where the acoustic resistance $\mathcal{R}$ and reactance $\mathcal{X}$ are functions of Mach number, width, and length. The predicted depth modes of this expression may be seen in figure 3 where equation (4) is plotted for all cases listed in table II. Note that the predicted spectra for cases 1 to 7 have similar shape but when the depth is halved, as in case 8, the predicted spectrum shows a significant change.

Recent investigations indicate that the noise produced by flow over a cavity has several regions of hydrodynamic resonance. These regions are dependent upon the cavity

length-to-depth ratio. When proper conditions exist for any of these resonances which have tonal characteristics, intense sound may be generated. Interaction between the hydrodynamic and acoustic models can cause significant amplifications of the pressure disturbances. Oscillatory response, however, is not a necessary condition for sound generation since acoustic radiation can occur when these resonances are not present but the response will be broadband and reduced in amplitude.

PRESENTATION OF RESULTS

Internal and External Pressure Measurements

Internal and external pressure measurements were made with the experimental arrangement described previously. The background noise, that is the noise produced by the flow over a flat plate without the cavity, is shown in figure 4. These data were measured at the location of sensor 4 which is directly over the front edge of the cavity.

The data taken at sensor 1 include both the dynamic fluid pressures inside the cavity and the acoustic pressures insonifying this surface. Although it is not clear whether the oscillating pressures measured at this location are representative of all periodic phenomena occurring within the cavity, the periodic phenomena occurring at this surface may be related to the external sound field.

Figure 5 shows the internal pressure spectra as measured at sensor 1 with the external or sound spectra measured directly over the cavity at location 4 for all cases listed in table II. Location 4 was chosen for this comparison; however, as will be shown later, the spectra of all farfield positions were similar, producing a monopolelike pattern. The background level is included to show the increase in noise produced by the cavity over that produced by a flat plate. This increase is considerable. In general the farfield sound spectra closely resemble the internal pressure spectra. Some internal pressure variations radiate sound more efficiently than others (figs. 5(a) and 5(d)) and some do not appear to radiate at all (fig. 5(b) at the 2000-Hz band). Several tones appear in some internal pressure spectra indicating several coexistent periodic phenomena or modes. The dominant mode occurs in the 1000-Hz band and appears to be the most efficient radiator. The higher frequency oscillations are much less efficient radiators.

In figures 5(a) to 5(f), representing cases 1 to 7, the cavity depth remains constant while the length and velocity vary. The frequency response remains a maximum in the 1000-Hz band except in figure 5(d) which will be discussed later. It therefore appears that this source phenomenon is controlled neither by velocity nor length. Recall that the source phenomena for equations (1) and (2) are both length and velocity dependent. When equations (3) and (4) are applied, only equation (4) seems to predict a resonance in this band as shown in figure 3.

The effect of varying the cavity length is shown in figures 5(a) to 5(c) where the cavity length is increasing while the depth and velocity are held constant. The maximum response remains in the 1000-Hz band, suggesting this response is not controlled by length, however, the amplitude decreases as the cavity length increases. The oscillatory response appearing in the 3150-Hz band shifts down in frequency to the 2000-Hz band as the length is increased, suggesting this response is controlled by length. However, this cavity response does not appear to radiate. A third tonal response occurs in the 4000-Hz band and does not seem to shift as cavity length is increased; however, the wide bandwidth of this frequency band precludes observing a frequency shift for the purpose of further identifying this response.

In figures 5(d) to 5(h) the velocity is twice the velocity of the previous cases. The effect of doubling the velocity can be seen by comparing figures 5(b) with 5(e) and 5(c) with 5(f). The amplitude of the external sound field increased from 14 to 20 dB above the cavity. In figures 5(d) to 5(g) the cavity length is increasing yielding a length-to-depth ratio from 1 to 2. The major amplitude response begins in the 3150-Hz band (fig. 5(d)) and shifts down to the 1000-Hz band (fig. 5(e)) as the length increases. However, as the length is increased further the maximum amplitude response remains in the 1000-Hz band (fig. 5(f)). It is believed that this response is controlled by the depth and that the response in the 3150-Hz band in figure 5(d) is the second depth mode of that observed in figures 5(a), (b), (c), (e), and (f). The second depth mode could have been excited by an amplitude response controlled by the cavity length in the vicinity of the 3150-Hz band for a length-to-depth ratio of 1. Figures 5(e) and 5(f) follow the same pattern as 5(b) and 5(c) in regard to the frequency shift of the second major amplitude response from the 3150-Hz and down to the 2000-Hz band as the cavity length is increased. This indicates that for a length-to-depth ratio of 1 this length-controlled response was likely to occur in the vicinity of the second depth mode shown in figure 3. As the length was increased from 6.35 cm to 8.9 cm in figures 5(d) and 5(e) the length excitation decreased in frequency and the cavity reverted to oscillating in the first depth mode. Therefore, in case 4 it is possible that an interaction or coupling of a length-controlled and depth-controlled phenomenon is observed, whereas in case 1, where the geometry is the same and the velocity is halved, this interaction or reinforcement does not occur. Operating in this coupled mode, although a high level is measured inside the cavity, it appears to be an inefficient radiator of sound. Figure 5(f) shows that the second major amplitude response in the 2000-Hz band, which has been associated with the cavity length, appears to radiate, however, not as efficiently as the major amplitude response associated with the cavity depth.

As the cavity length is increased further, figure 5(g) shows that the first depth mode diminishes and the primary amplitude response becomes that of the length mode which has shifted down in frequency from the 2000-Hz band to the 1600-Hz band.

In figure 5(h) the length remained the same as in figure 5(g) while the depth was halved. The spectra became more broadband and an upward shift in frequency occurs. The pressure

response calculated using equation (4) is shown for this case in figure 3. This predicted response is more broadband and peaks in the 2000-Hz band near the 1600-Hz band (see fig. 3). This is also observed experimentally in figure 5(h) indicating that the maximum response amplitude in this case may be depth related.

Comparison of Predicted and Measured Response Frequency

Because of the lack of resolution of the 1/3-octave filter bands at the frequencies of interest, it is not possible to determine conclusively which source mechanism or corresponding equation is suitable for predicting the frequencies of cavity oscillation obtained in this experiment. This, however, does not preclude obtaining information from a comparison of theory and experiment. This comparison is made to evaluate how consistent each equation is in predicting the experimentally observed resonance frequency within the 1/3-octave bandwidth as the velocity, length, and depth are varied.

Table III lists the peak response frequencies predicted by equations (1) to (4) for the test conditions listed in table II. Table III is truncated in most cases above about 4000 Hz because no response frequencies were measured above this frequency. Table IV presents a comparison of the predicted frequencies represented by the mode numbers taken from table III with those obtained experimentally. Column 2 of table IV contains the frequency range in which an oscillatory cavity response was obtained. The range of frequencies given in column 2 results from the uncertainty of exact location of the response frequency within the 1/3-octave band. Column 3 lists the controlling dimension for the particular mode of oscillation as assigned and discussed previously. The internal-pressure-response frequencies (sensor 1) are used since equations (1) to (4) are applicable to internal pressure fields only. Columns 4 to 7 list the modes of the equation that predict a major response frequency with the range listed in column 2.

The dominant or maximum amplitude response occurring in the 1000-Hz band was found experimentally to be depth related. Equation (4), which is the only equation that uses the depth dimension in calculating the pressure response of open cavities, predicts a maximum pressure response in the vicinity of 1050 Hz for cases 1 to 7. As can be seen in figures 5(a) to 5(f) excluding 5(d), the 1000-Hz band contains the major amplitude response which was related to the depth. For case 8, where the depth is halved, equation (4) again correctly predicts both the shape (broadband) and maximum frequency for this case (see figs. 3 and 5(h)).

For each of the cases where a length-controlled response was determined from the data, equations (1) and (2) predict one or several possible modes for their respective phenomena. This results from the wide filter bandwidth. The modal numbers of equation (1) and (2) are close in every case and so are the frequencies associated with those modal numbers (see table III); however, this is not always the case. Equation (3), which computes the frequencies

of the width and length modes of the acoustic resonator model, was found to be unsuitable for predicting oscillation frequencies of the cavity. The first width mode was above 6000 Hz; therefore, only the length modes of equation (3) are listed for comparison in column 6 of table IV.

Effect of Altering the Boundary Layer

In one series of tests a rough turbulence-generating strip was placed in the constant area section at the bottom edge of the nozzle, upstream of the plate containing the cavity (see fig. 1). The purpose of this series was to investigate the noise-reduction merits of this device over a range of configurations. The turbulence strip consisted of No. 40 grit particles and was 1.27 cm wide. The effect of altering the boundary layer on the internal and acoustic (sensor 4) pressure spectra is shown in figure 6. The internal as well as the external pressure spectra are modified to some extent by this additional boundary-layer turbulence. As in the previous series of cases, where the roughness element was absent, the external (or acoustic) pressure spectra are patterned after the internal pressure spectra when the roughness element is present.

In figures 6(a) to 6(c) the velocity is fixed at 43 m/sec and the length is increasing. The amount of sound reduction realized in the 1000-Hz band decreases as the length increases. The internal oscillatory pressure responses associated with the length are more uniformly attenuated inside the cavity as the length increases; however, at this velocity the length-mode pressure disturbance does not appear to radiate as sound.

In figures 6(d) to 6(h) the velocity is twice that of figures 6(a) to 6(c). Figure 6(d) indicates that the added turbulence excites a cavity response in the 1250-Hz band as also seen in figure 6(a). This response is not predicted by equation (4) and is associated with a length-controlled phenomenon. The second depth mode observed in the 3150-Hz band is greatly attenuated (20 dB) by the added turbulence.

Figures 6(e) and 6(f) show that the added turbulence is less effective in reducing the amplitude of the depth-controlled response as the length is increased. In comparing figures 6(b) and 6(c) with 6(e) and 6(f) it appears that at the higher velocity the amount of noise reduction obtained is decreased, perhaps owing to the decrease of the turbulent-boundary-layer thickness with increasing velocity.

Inside the cavity the amplitude of the length-controlled response is increased in figure 6(e) and decreased in figure 6(f). In figures 6(e) to 6(h) the roughness element is seen to effect the spectra in several different ways. In figure 6(e) the roughness element appears to increase the internal dynamic pressure, slightly reducing the radiated sound. In figures 6(f) and 6(g) there is a reduction in the tonal and broadband parts of the spectra outside the cavity, respectively. Figure 6(h) represents the pressure spectra measured from a relatively shallow cavity. The amount of noise reduction realized here is slight.

Directivity

In figures 7(a) to 7(h) are plotted the directivity patterns in the X-Z ($\phi = 0^o$) and Y-Z ($\phi = 90^o$) coordinate planes for all cases listed in table II, with and without the roughness element. The open and solid symbols represent the level with and without the roughness element, respectively. The directivity patterns in figures 7(a) to 7(f) are composed of the amplitudes of the 1/3-octave bands in which major cavity resonances occurred. Figures 7(g) and 7(h) represent the sound pressure level from 800 Hz to 5000 Hz since the cavity response in these configurations was more random in character. Since the measured directivity patterns were symmetrical, the levels at locations 2 and 6 were combined and represented at $\phi = 0^o$, $\theta = 90^o$. Similarly the levels at locations 3 and 5 were combined and represented at $\phi = 0^o$, $\theta = 45^o$. The levels at locations 7 and 9 were combined and represented at $\phi = 90^o$, $\theta = 90^o$. Neither of these microphones was located in the $\phi = 90^o$ plane as seen in figure 1. Their combined level is shown at $\phi = 90^o$ for ease of display. To determine the directivity, shear-layer refraction and attenuation corrections have been made on all data as suggested in reference 19. Incidentally, according to reference 19, no corrections are required for sensor 4. Recall that the sensor at location 4 was used in the previous discussions. The amplitude corrections varied from 0 to 3 dB and the refraction corrections were 10^o for 43 m/sec and 20^o for 86 m/sec at position 8.

Figures 7(a) to 7(c) represent the low-velocity case in which the 1000-Hz band was the dominant response mode and only major response measured outside the cavity. The maximum sound level occurs above the cavity and decreases to the side. In each case the roughness element significantly reduced the sound level but its effectiveness decreased with increasing length. The directivity is not considerably altered when the roughness element is used.

Figures 7(d) to 7(f) show the directivity of each of the radiated cavity oscillatory responses for the higher-velocity case. The directivity remains circular with slight decrease in the X-Y plane. As seen previously (fig. 6(d) and also in fig. 7(d)) the increased roughness decreased the amplitude of the response in the 3150-Hz band and increased the level in the 1250-Hz band by approximately the same amount above the cavity. The maximum amplitude in this 3150-Hz band is not found above the cavity, as seen in every other case, but rather to the side. When the roughness element was added, the directivity pattern reverted to a more circular pattern, the attenuation being greatest in the $\theta = 45^o$ direction.

The directivities for cases 7 and 8 are shown in figures 7(g) and 7(h). Although the spectra were more random, the directivity patterns show a similar shape to that obtained with tonal spectra. The effect of the roughness element in reducing the noise is small and it does not appear to alter the directivity pattern significantly.

In all above cases except that represented by case 4 the cavity had a radiation pattern that is close to that of a simple source. This was observed in reference 7 for low velocities

with the aid of schlieren photography. However, the author notes that at velocities approaching Mach 1 the radiation pattern appears more directional.

The directivity patterns suggest that the cavity is behaving as a monopole or simple source; however, the deviations from a circular pattern may be caused by the presence of a dipole oriented in the Z-axis direction.

CONCLUDING REMARKS

Several periodic phenomena, whether length or depth controlled, can simultaneously occur in a flow-excited cavity when the length-to-depth ratio is about 1. These phenomena raise the noise level considerably over that of flow over a flat plate. The lower-frequency phenomena radiate more efficiently as sound. This efficiency, however, may be attributed to the type of oscillation, namely depth controlled, rather than the frequency of oscillation. The comparison of predicted and measured response frequencies indicates that in deeper cavities an acoustic resonator model is appropriate for predicting some of the observed peaks. The oscillating shear-layer and feedback models provide a multitude of predicted response frequencies; however, it is believed that their merit lies in the higher Mach number range. Using a roughness element to increase the boundary-layer thickness upstream of the cavity was found to be effective in reducing the radiated noise. As velocity and/or cavity length increased this addition of a roughness element became less effective in reducing the radiated noise. The effect of this device on the radiated sound spectrum varied. In one case no noise reduction was realized, in another a change in spectral shape was achieved; however, no net reduction in overall noise was realized. For the cavity dimensions and flow velocities reported herein, the directivity pattern remained approximately circular or that of a combined monopole and dipole source, except in the case where a length- and depth-controlled mode were coupled. The roughness element did not significantly alter the directivity patterns.

Langley Research Center
National Aeronautics and Space Administration
Hampton, Va. 23665
October 15, 1975

REFERENCES

1. Gibson, John S.: The Ultimate Noise Barrier – Far Field Radiated Aerodynamic Noise. Inter-Noise 72 Proceedings, Malcolm J. Crocker, ed., Inst. Noise Contr. Eng., c.1972, pp. 332-337

2. Blumenthal, V. L.; Streckenbach, J. M.; and Tate, R. B.: Aircraft Environmental Problems. AIAA Paper No. 73-5, Jan. 1973.

3. Healy, Gerald J.: Measurement and Analysis of Aircraft Far-Field Aerodynamic Noise. NASA CR-2377, 1974.

4. Gibson, John S.: Non-Engine Aerodynamic Noise Investigation of a Large Aircraft. NASA CR-2378, 1974.

5. Hardin, Jay C.; Fratello, David J.; Hayden, Richard E.; Kadman, Yoran; and Africk, Steven: Prediction of Airframe Noise. NASA TN D-7821, 1975.

6. Nyborg, Wesley L.: Self-Maintained Oscillations of the Jet in a Jet-Edge System. I. J. Acoust. Soc. America, vol. 26, no. 2, Mar. 1954, pp. 174-182.

7. Krishnamurty, K.: Acoustic Radiation From Two-Dimensional Rectangular Cutouts in Aerodynamic Surfaces. NACA TN 3487, 1955.

8. Roshko, Anatol: Some Measurements of Flow in a Rectangular Cutout. NACA TN 3488, 1955.

9. Dunham, William H.: Flow-Induced Cavity Resonance in Viscous Compressible and Incompressible Fluids. Fourth Symposium on Naval Hydrodynamics – Propulsion Hydroelasticity, ACR-92, Aug. 1962, pp. 1057-1081.

10. Harrington, M. C.; and Dunham, W. H.: Studies of the Mechanism for the Flow-Induced Cavity Resonance. J. Acoust. Soc. America, vol. 32, no. 7, July 1960, p. 921.

11. Plumblee, H. E.; Gibson, J. S.; and Lassiter, L. W.: A Theoretical and Experimental Investigation of the Acoustic Response of Cavities in an Aerodynamic Flow. WADD-TR-61-75, U.S. Air Force, Mar. 1962.

12. Maull, D. J.; and East, L. F.: Three-Dimensional Flow in Cavities. J. Fluid Mech., vol. 16, pt. 4, Aug. 1963, pp. 620-632.

13. Rossiter, J. E.: Wind-Tunnel Experiment on the Flow Over Rectangular Cavities at Subsonic and Transonic Speeds. R. & M. No. 3438, British A.R.C., Oct. 1964.

14. Spee, B. M.: Wind Tunnel Experiments on Unsteady Cavity Flow at High Subsonic Speeds. Separated Flows, Part II, AGARD CP No. 4, May 1966, pp. 941-974.

15. East, L. F.: Aerodynamically Induced Resonance in Rectangular Cavities. J. Sound & Vib., vol. 3, no. 3, May 1966, pp. 277-287.

16. Heller, H. H.; Holmes, D. G.; and Covert, E. E.: Flow-Induced Pressure Oscillations in Shallow Cavities. J. Sound & Vib., vol. 18, no. 4, Oct. 1971, pp. 545-553.

17. Heller, Hanno H.; and Bliss, Donald B.: The Physical Mechanism of Flow-Induced Pressure Fluctuations in Cavities and Concepts for Their Suppression. AIAA Paper 75-491, Mar. 1975.

18. Kadman, Y.; and Hayden, R. E.: Design and Performance of High-Speed Free-Jet Acoustic Wind Tunnel. AIAA Paper 75-531, Mar. 1975.

19. Amiet, Roy K.: Correction of Open Jet Wind Tunnel Measurements for Shear Layer Refraction. AIAA Paper 75-532, Mar. 1975.

TABLE I.- SENSOR LOCATIONS

Sensor	θ, deg	ϕ, deg
1	Located in the cavity	
2	90	0
3	45	0
4	0	0
5	45	180
6	90	180
7	90	45
8	45	90
9	90	135

TABLE II.- TEST CONDITIONS

Case	L, cm	D, cm	W, cm	L/D	V, m/sec
1	6.35	6.35	2.54	1.0	43
2	8.9	↓	↓	1.4	↓
3	10.16	↓	↓	1.6	↓
4	6.35	↓	↓	1.0	86
5	8.9	↓	↓	1.4	↓
6	10.16	↓	↓	1.6	↓
7	12.7	↓	↓	2.0	↓
8	12.7	3.18	↓	4.0	↓

TABLE III.- PREDICTED FREQUENCIES OF CAVITY OSCILLATION

Mode number, m	Frequency in Hz for case							
	1	2	3	4	5	6	7	8
Nyborg/Spee prediction (eq. (1))								
1	290	207	181	581	415	363	290	290
2	705	503	441	1410	1006	881	705	705
3	1114	794	696	2227	1589	1392	1114	1 114
4	1520	1085	950	3041	2170	1901	1521	1 521
5	1928	1375	1205	3855	2751	2410	1928	1 928
6	2334	1666	1459	4669	3331	2918	2334	2 334
7	2741	1956	1713	5482	3911	3426	2741	2 741
8	3148	2246	1967	6294	4491	3934	3147	3 147
9	3553	2535	2221	7108	5071	4442	3553	3 553
10	3960	2826	2475	7920	5651	4950	3960	3 960
11	4367	3116	2729					
12	4773	3405	2983					
13	5179	3695	3237					
Rossiter/Heller prediction (eq. (2))								
1	268	192	168	504	360	315	252	252
2	626	447	391	1176	840	735	588	588
3	984	703	615	1847	1320	1155	924	924
4	1342	958	839	2519	1800	1575	1260	1 260
5	1700	1214	1062	3191	2280	1994	1596	1 596
6	2057	1470	1286	3863	2759	2414	1931	1 931
7	2415	1725	1510	4534	3239	2834	2267	2 267
8	2773	1981	1733	5206	3719	3254	2603	2 603
9	3131	2236	1957	5878	4199	3674	2939	2 939
10	3490	2492	2180	6550	4678	4094	3275	3 275
11	3846	2747	2404	7276	5191	4548	3638	3 638
12	4204	3003	2628	7953	5674	4971	3977	3 977
13	4562	3259	2851	8630	6157	5394	4315	4 315
14	4920	3514	3075	9306	6640	5817	4653	4 653
15	5278	3770	3299		7123	6240	4992	4 992
16	5636	4025	3422		7606	6663	5330	5 330
17	6026	4280	3845		8089	7096	5669	5 669
18	6386	4536	3969			7509	6007	6 007
19	6746	4792	4193				6346	6 346
Acoustic resonator prediction (eq. (3), length mode)								
1	2712	1937	1695	2712	1937	1695	1356	1 356
2	5424	3874	3390	5424	3874	3390	2712	2 712
3	8136	5811	5085	8136	5811	5085	4068	4 068
Acoustic resonator prediction (eq. (3), width mode)								
1	6780	6780	6780	6780	6780	6780	6780	6 780
Plumblee, Gibson, and Lassiter prediction (eq. (4), depth mode)								
1	1090	1050	1050	1060	1055	1052	1040	1 845
2	3810	3760	3760	3780	3760	3760	3750	7 266
3	6500	6500	6450	6500	6500	6470	6450	12 590

TABLE IV.- COMPARISON OF PREDICTED AND EXPERIMENTALLY OBTAINED FREQUENCIES

Case	Experimental		Mode number predicted by –			
	Frequency range containing cavity response, Hz	Controlling dimension	Equation (1)	Equation (2)	Equation (3)	Equation (4)
1	900 to 1100	D	3	3	---	1
	2850 to 3590	L	8, 9	9, 10	---	---
2	900 to 1100	D	4	4	---	1
	1780 to 2500	L	7, 8	8, 9, 10	---	---
	3570 to 4490	---	13, 14, 15	15, 16, 17	2	2
3	900 to 1100	D	4	5	---	1
	1780 to 2240	L	8, 9	9, 10	---	---
	3570 to 4490	---	15, 16, 17	16, 17, 18, 19, 20	---	2
4	1100 to 1400	---	2	2	---	---
	2850 to 3590	L,D	4	5	---	---
5	900 to 1100	D	2	---	---	1
	2230 to 2850	L	5	5, 6	---	---
	3560 to 4490	---	7, 8	8, 9	2	2
6	900 to 1100	D	---	---	---	1
	1780 to 2240	L	4	5	---	---
	3570 to 4490	---	8, 9	9, 10	---	2
7	1425 to 1780	L	4	5	---	---
	2850 to 3590	---	8, 9	9, 10	---	---
8	1780 to 2240	D	5	6, 7	---	1

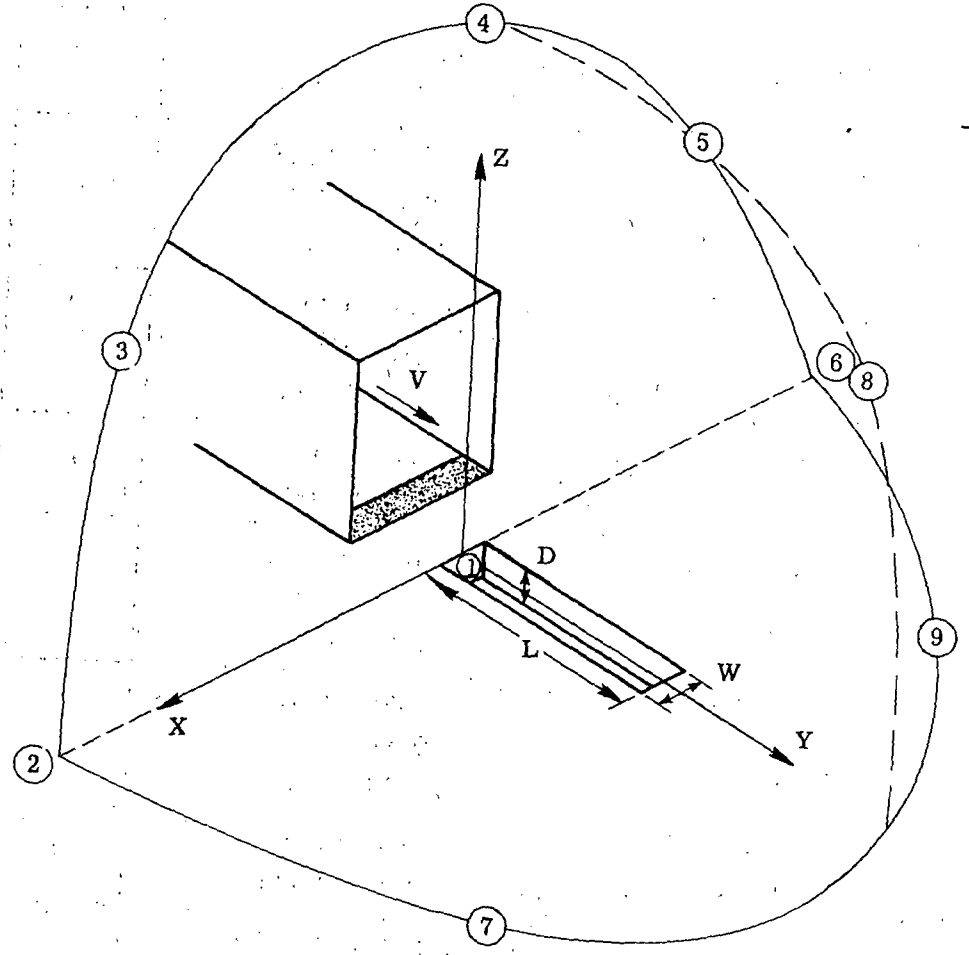

(a) Perspective view.

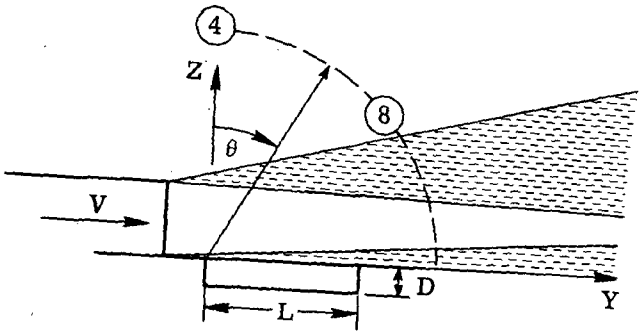

(b) Side view $\phi = 90^{o}$.

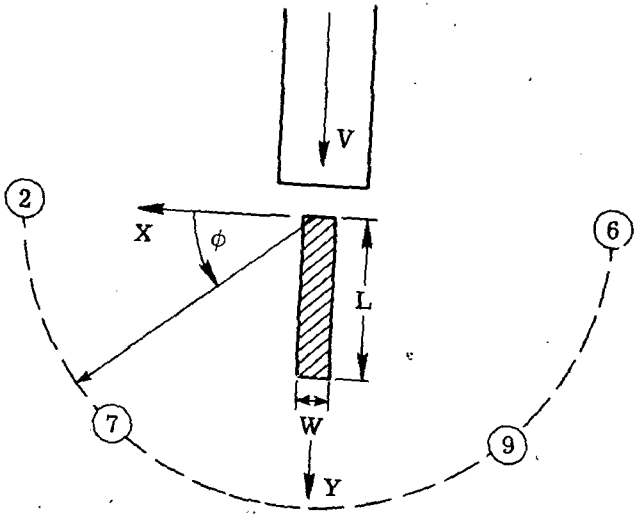

(c) Plan view $\theta = 90^{o}$.

Figure 1.- Experimental arrangement for cavity noise experiment. Numbers refer to sensor positions.

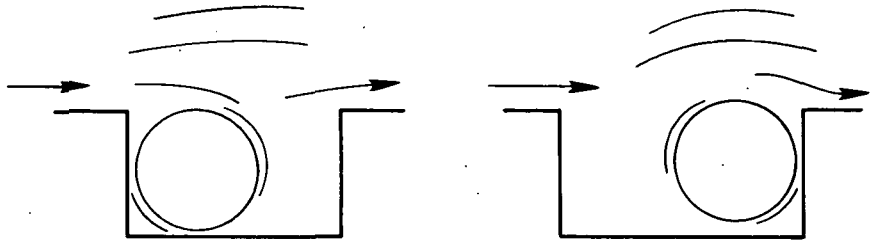

(a) Captive-vortex model.

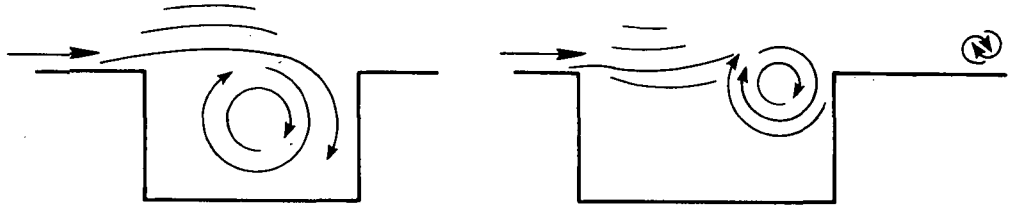

(b) Shear-layer oscillation associated with equation (1).

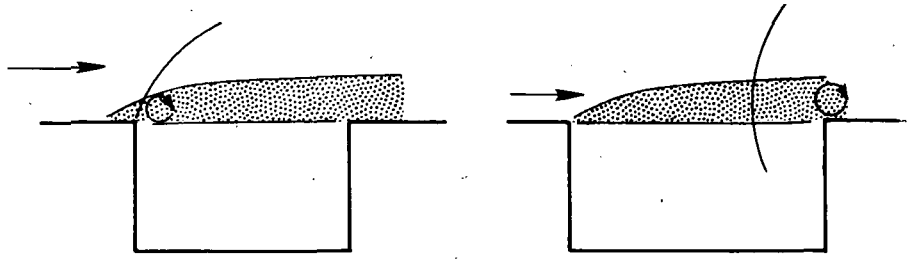

(c) Feedback model associated with equation (2).

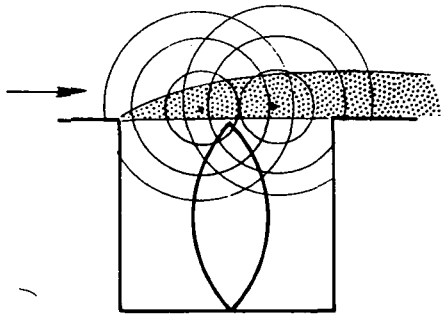

(d) Acoustic resonator (organ pipe) associated with equation (4).

Figure 2.- Proposed cavity noise sources.

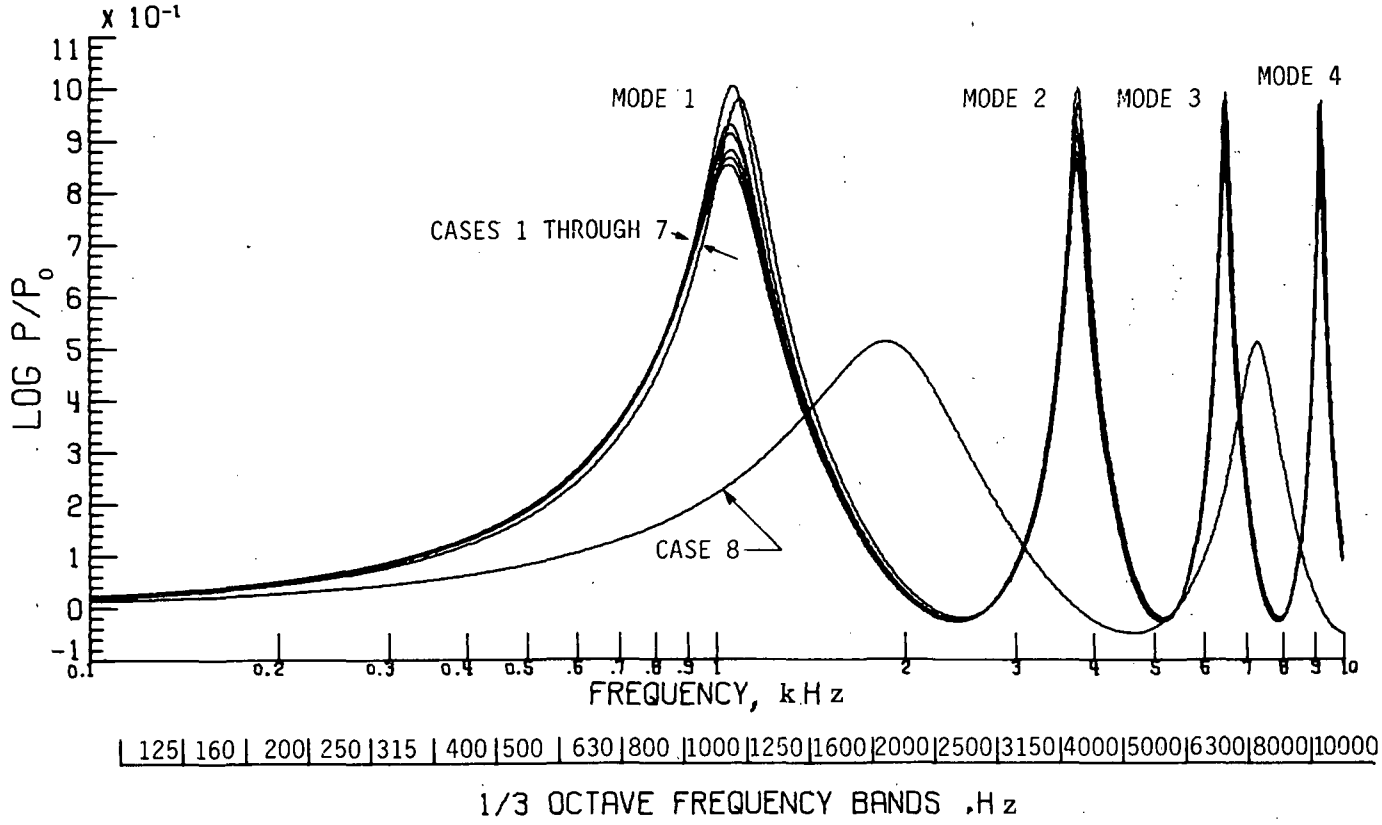

Figure 3.- Depth-mode pressure response (eq. (4)).

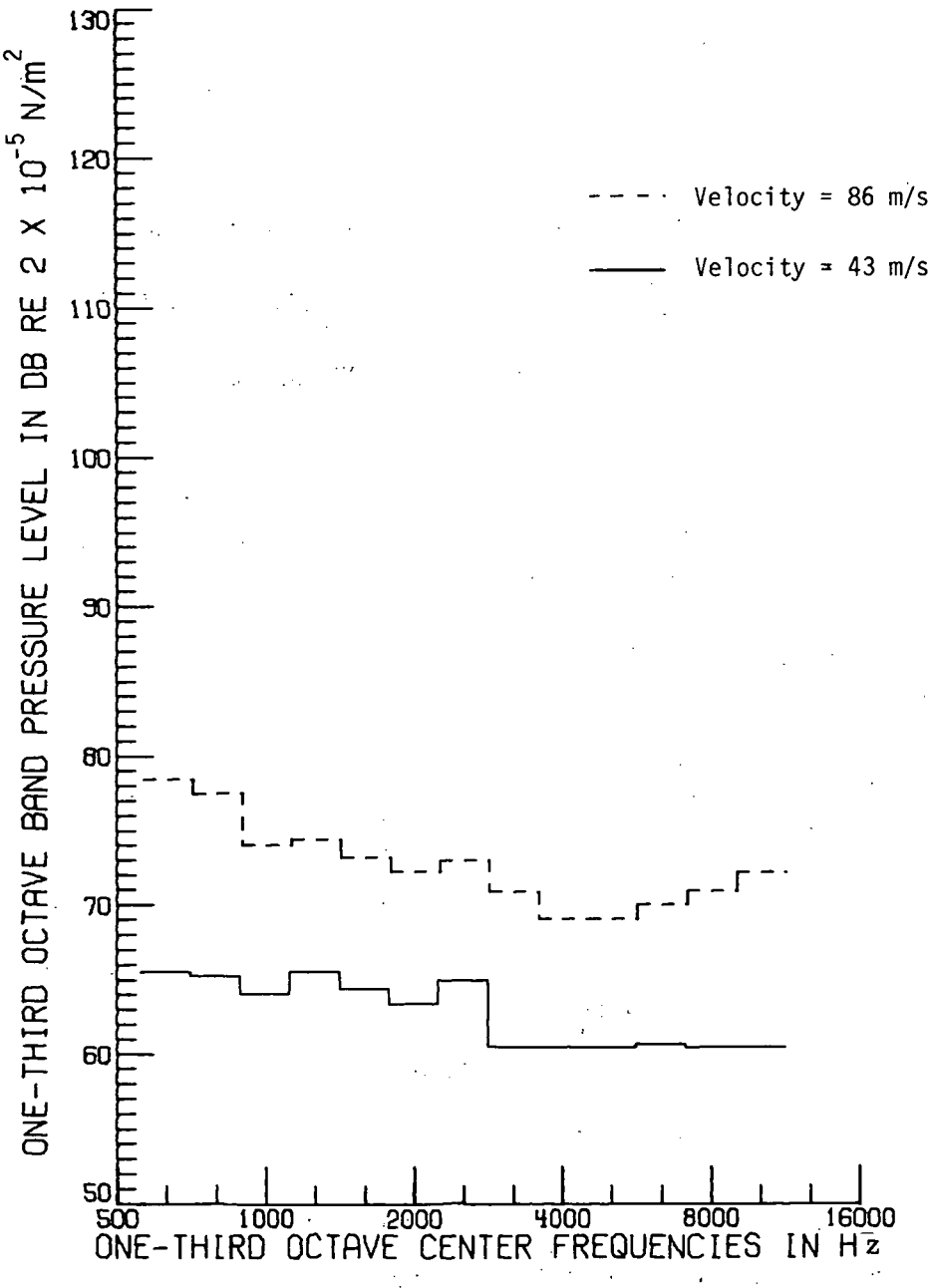

Figure 4.- Background noise recorded at location 4.

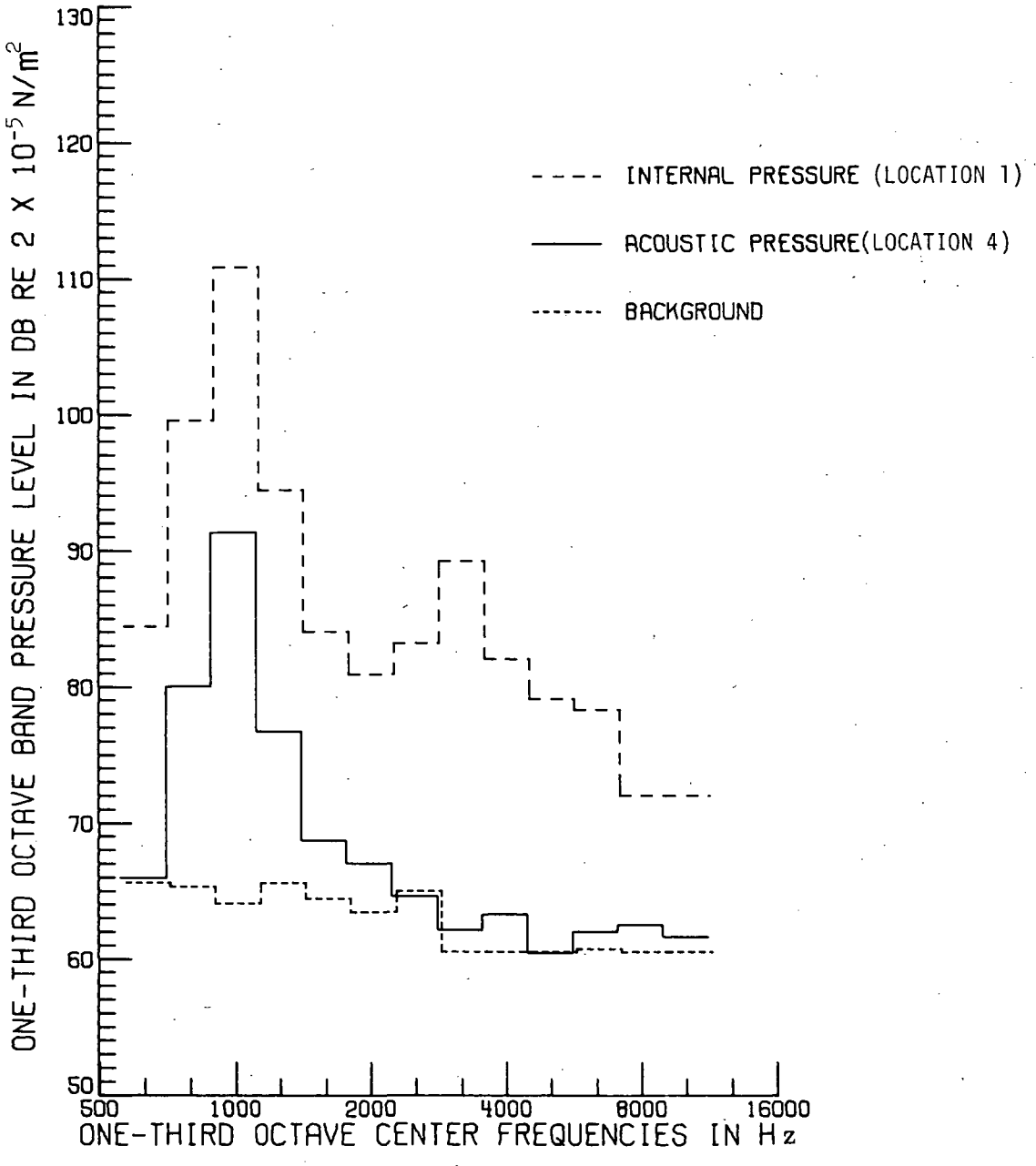

(a) Case 1. V = 43 m/sec; L/D = 1.

Figure 5.- Comparison of internal and external pressure spectra.

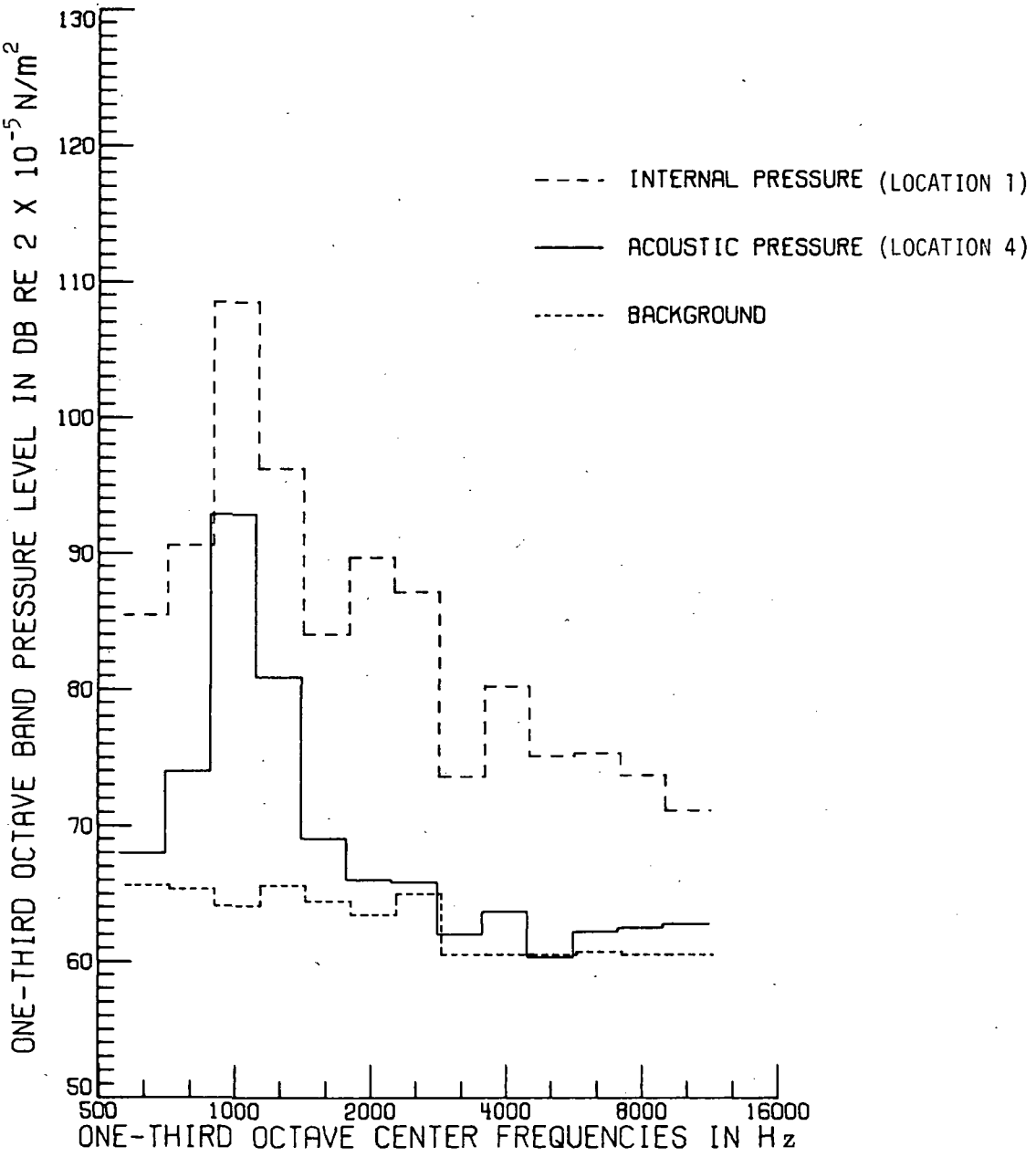

(b) Case 2. V = 43 m/sec; L/D = 1.4.

Figure 5.- Continued.

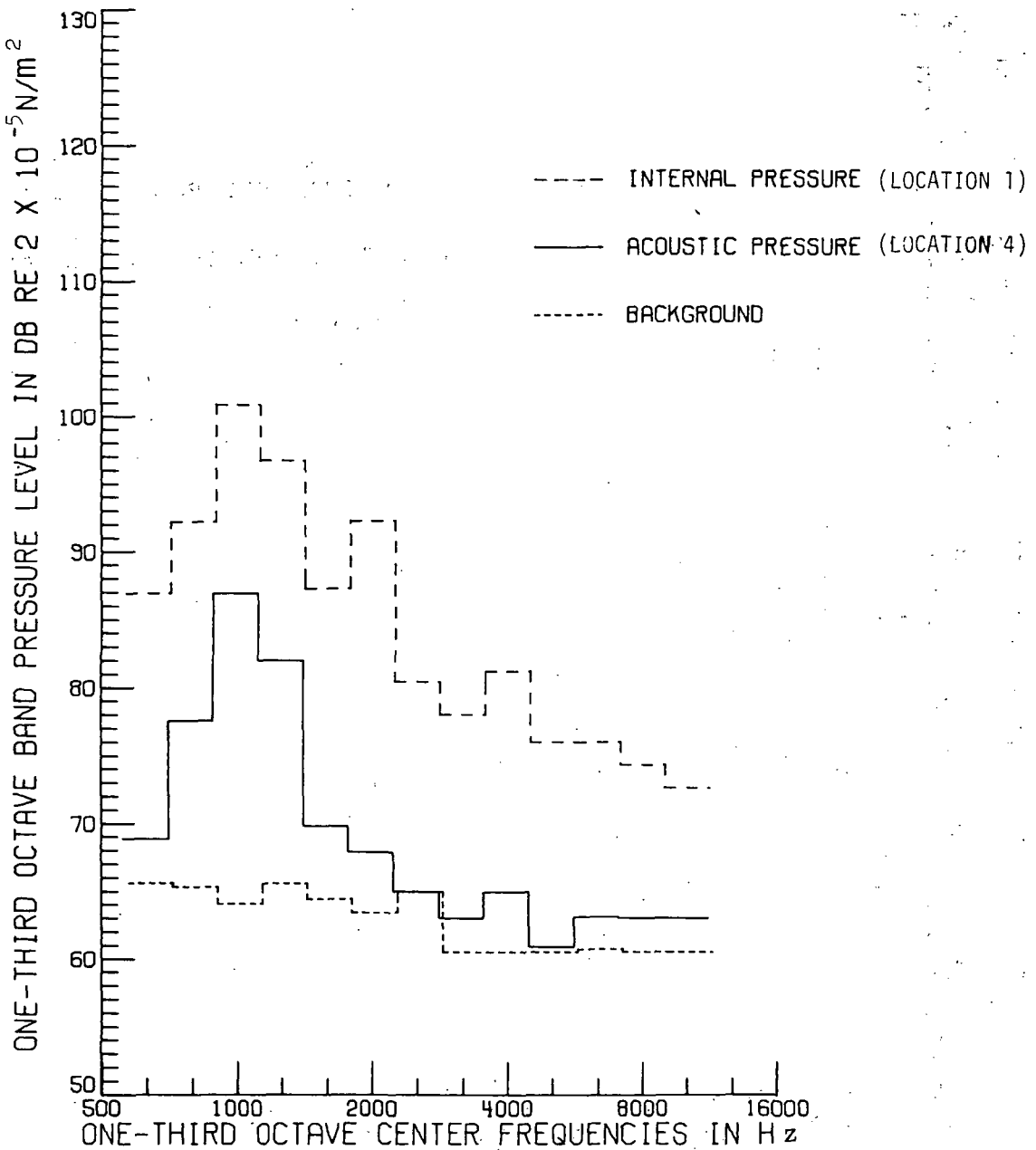

(c) Case 3. V = 43 m/sec; L/D = 1.6.

Figure 5.- Continued.

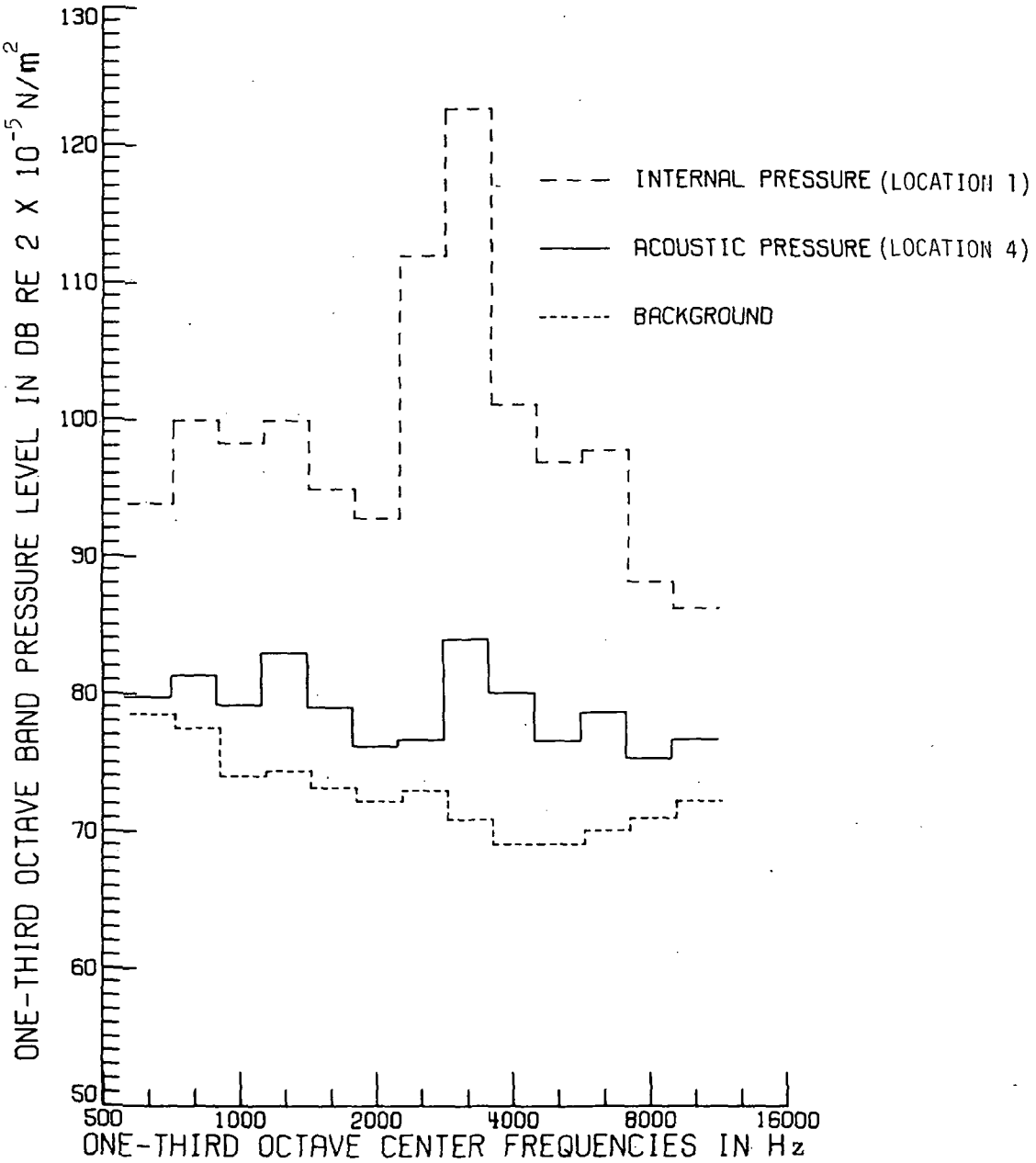

(d) Case 4. V = 86 m/sec; L/D = 1.

Figure 5.- Continued.

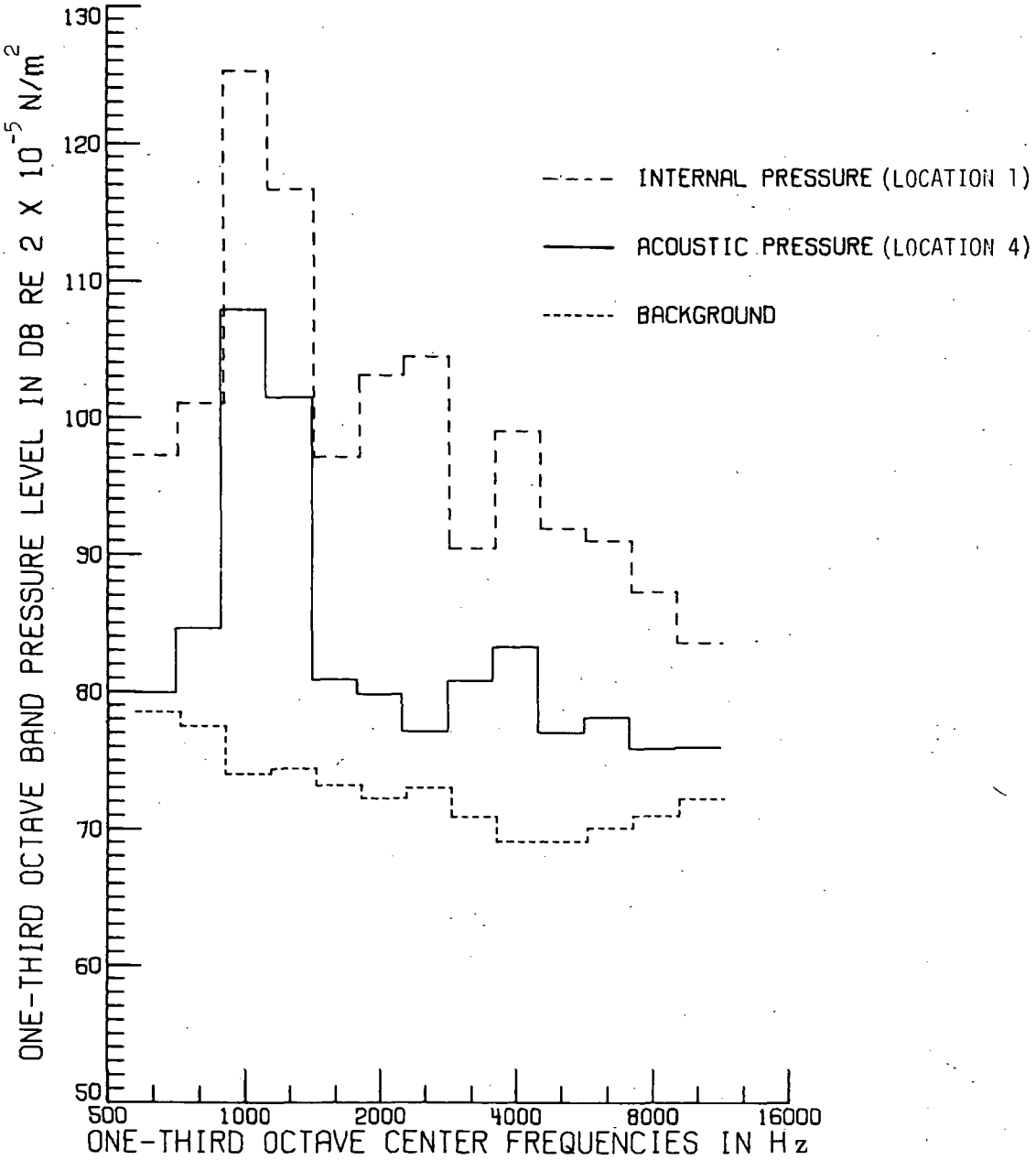

(e) Case 5. V = 86 m/sec; L/D = 1.4.

Figure 5.- Continued.

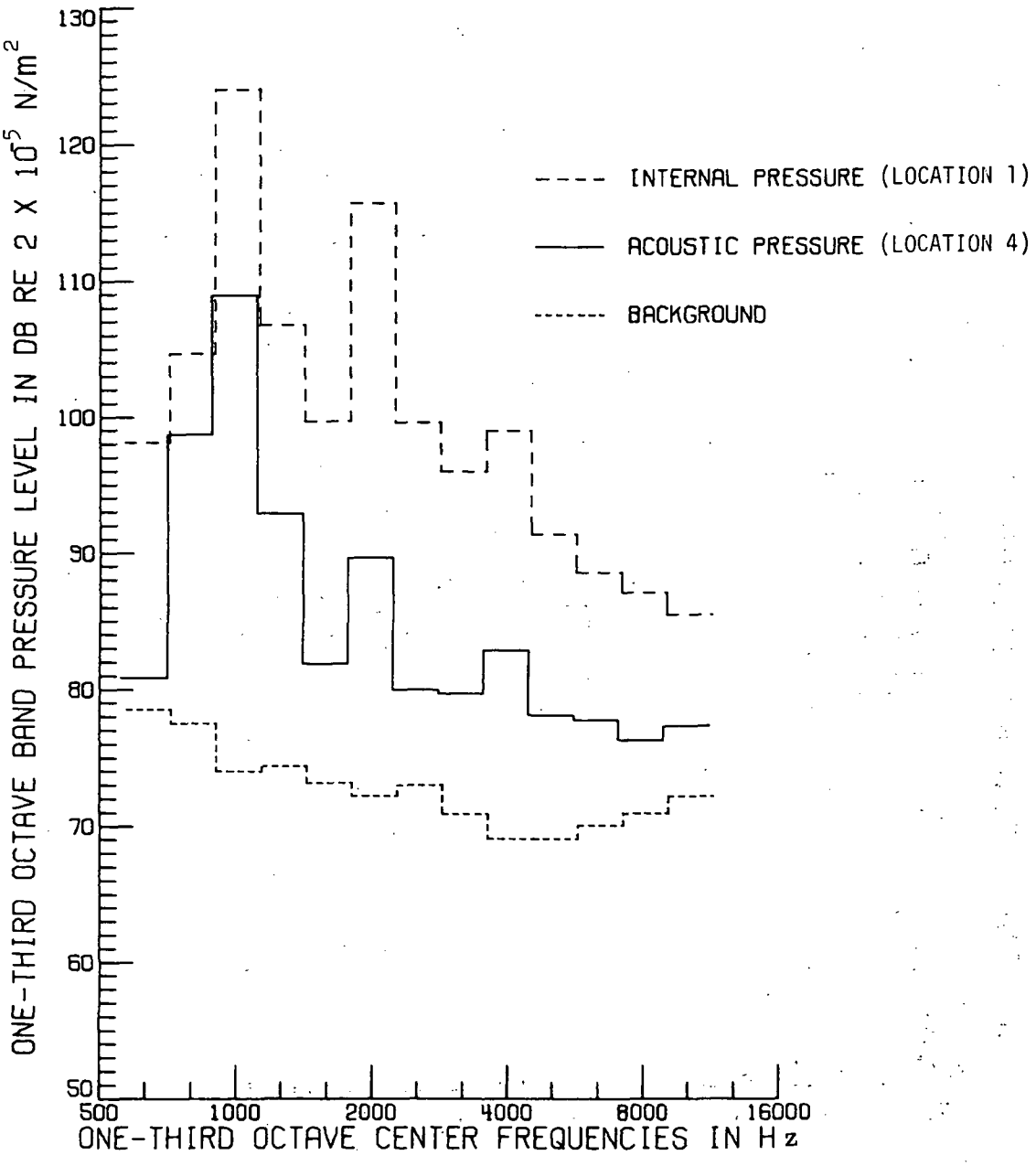

(f) Case 6. V = 86 m/sec; L/D = 1.6.

Figure 5.- Continued.

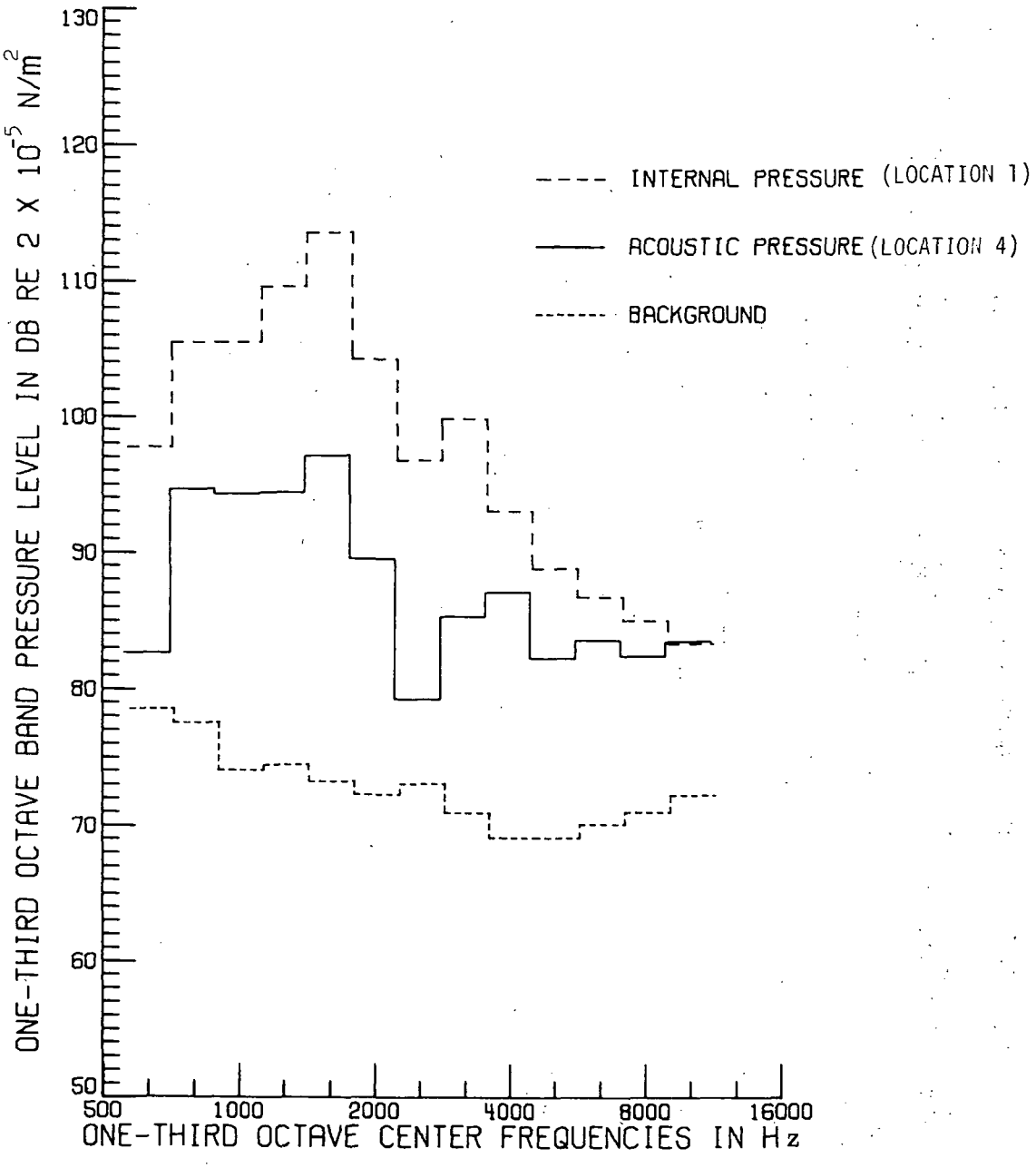

(g) Case 7. V = 86 m/sec; L/D = 2.

Figure 5.- Continued.

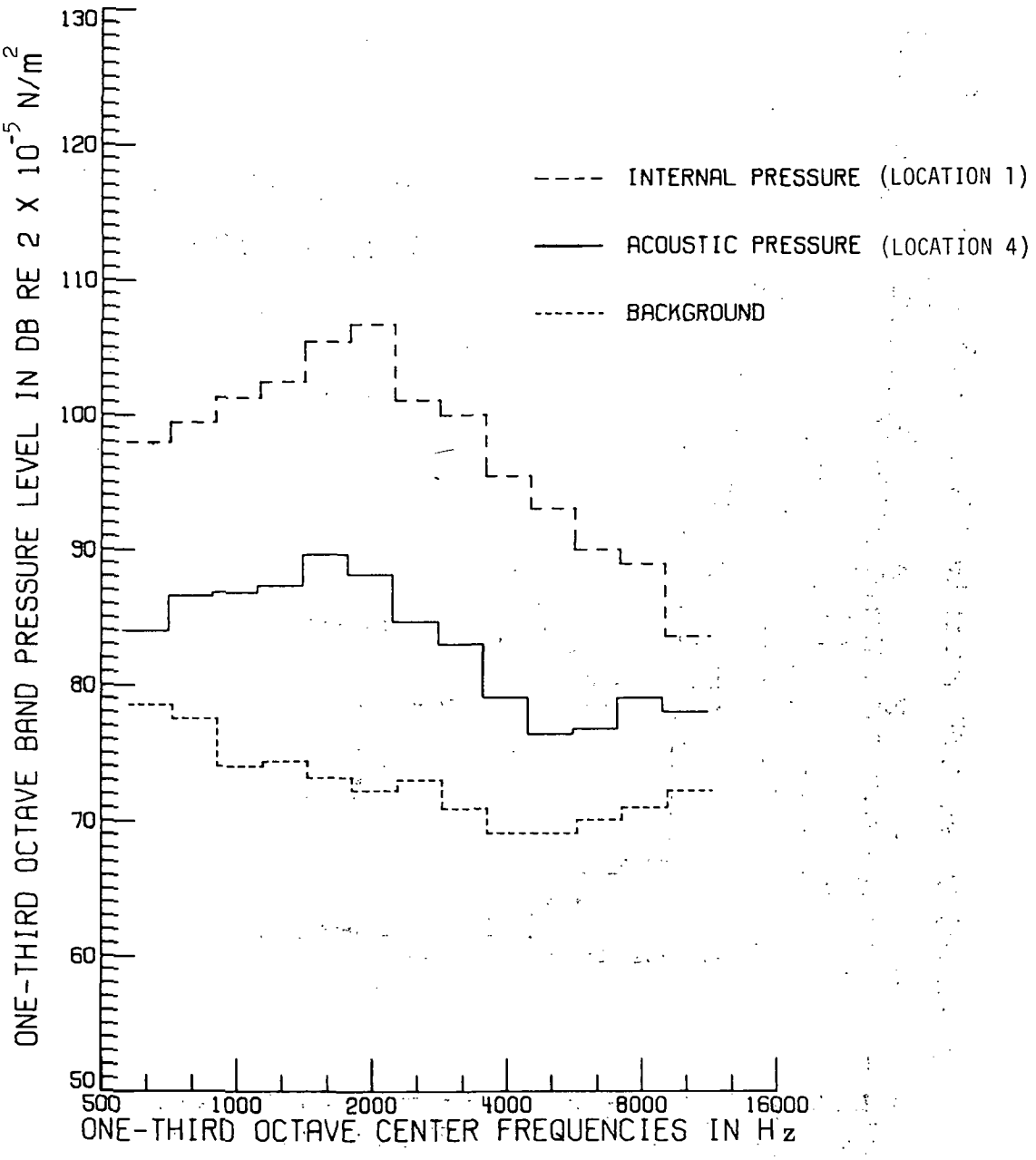

(h) Case 8. V = 86 m/sec; L/D = 4.

Figure 5.- Concluded.

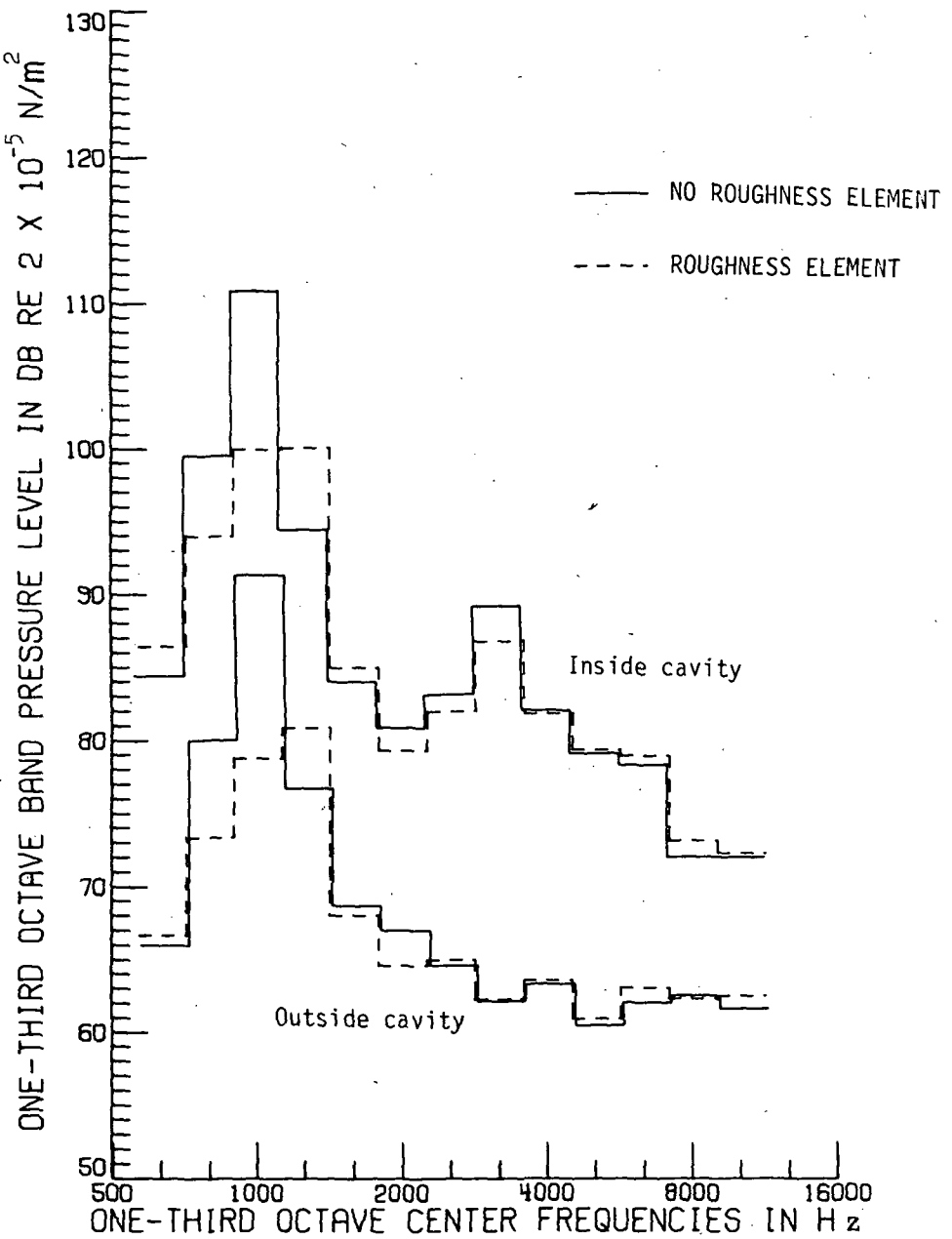

(a) Case 1. V = 43 m/sec; L/D = 1.

Figure 6.- Effect of roughness element.

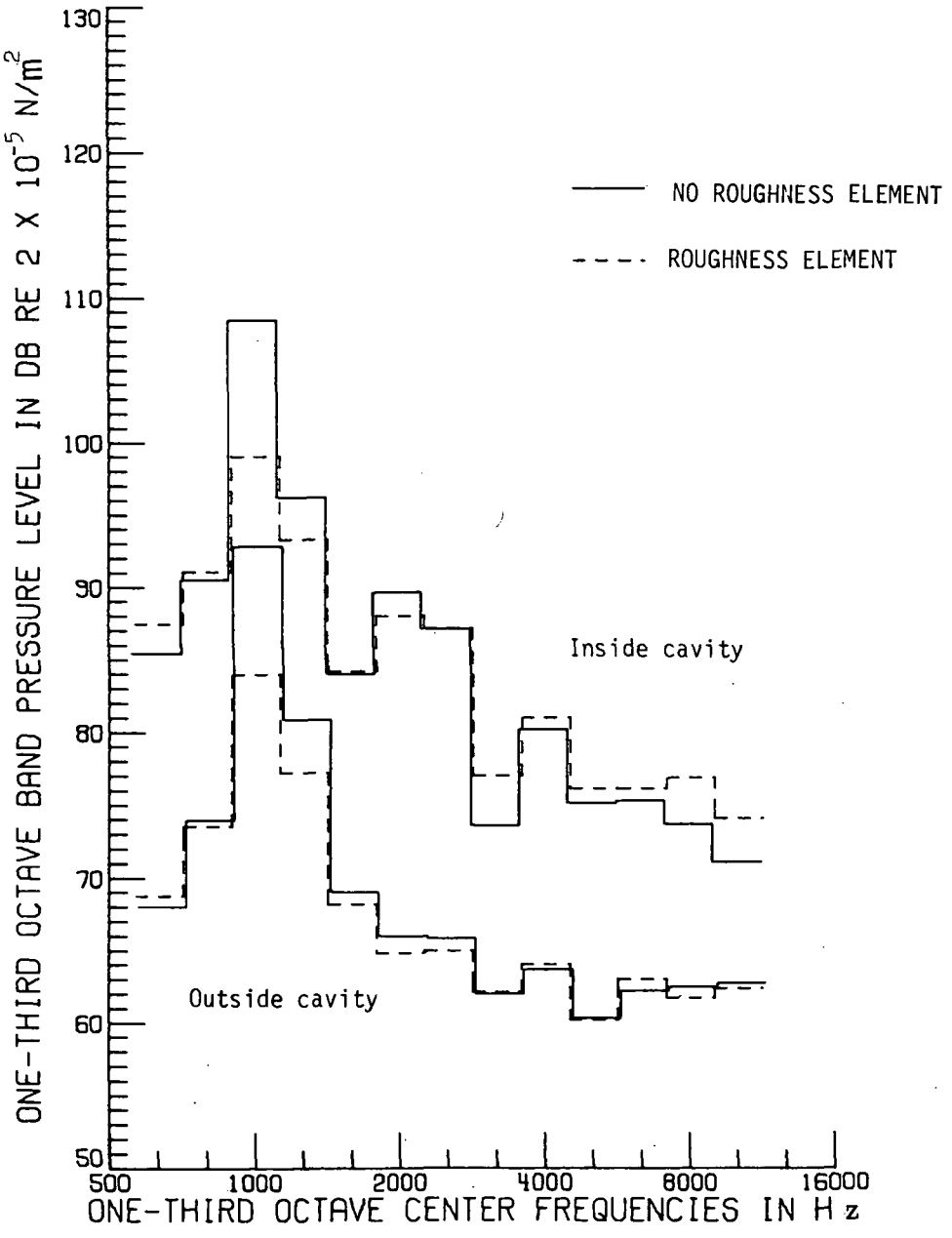

(b) Case 2. V = 43 m/sec; L/D = 1.4.

Figure 6.- Continued.

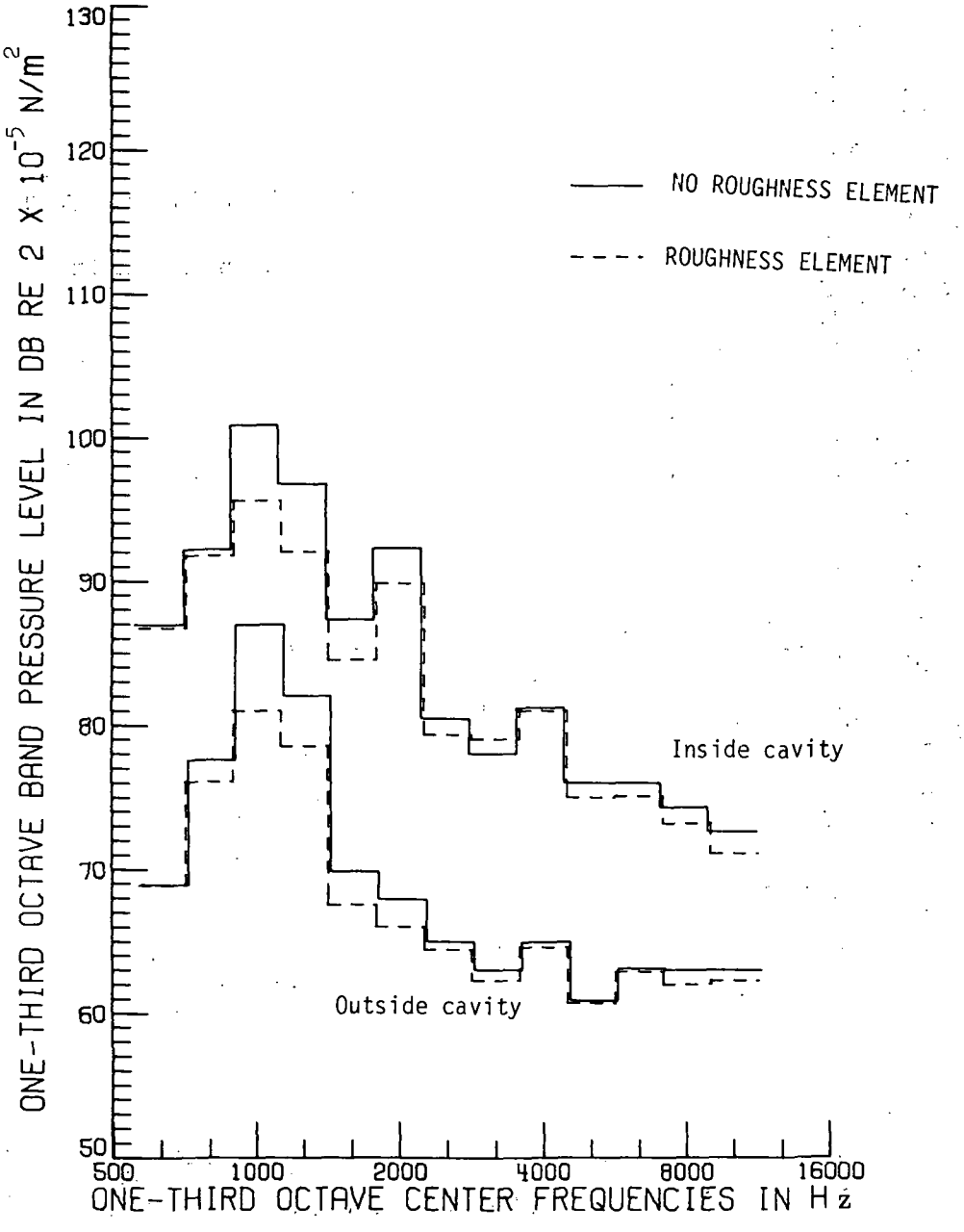

(c) Case 3. V = 43 m/sec; L/D = 1.6.

Figure 6.- Continued.

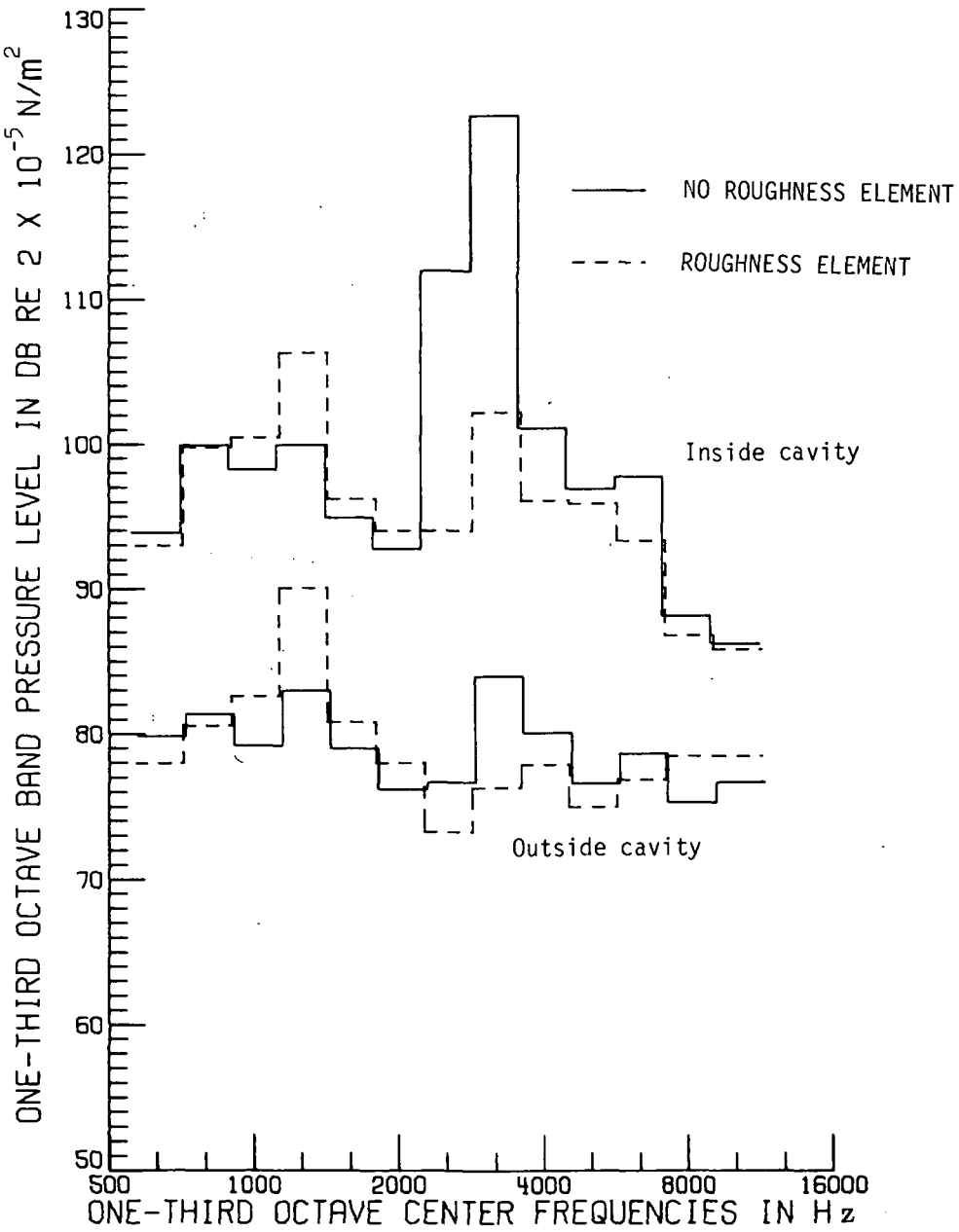

(d) Case 4. V = 86 m/sec; L/D = 1.

Figure 6.- Continued.

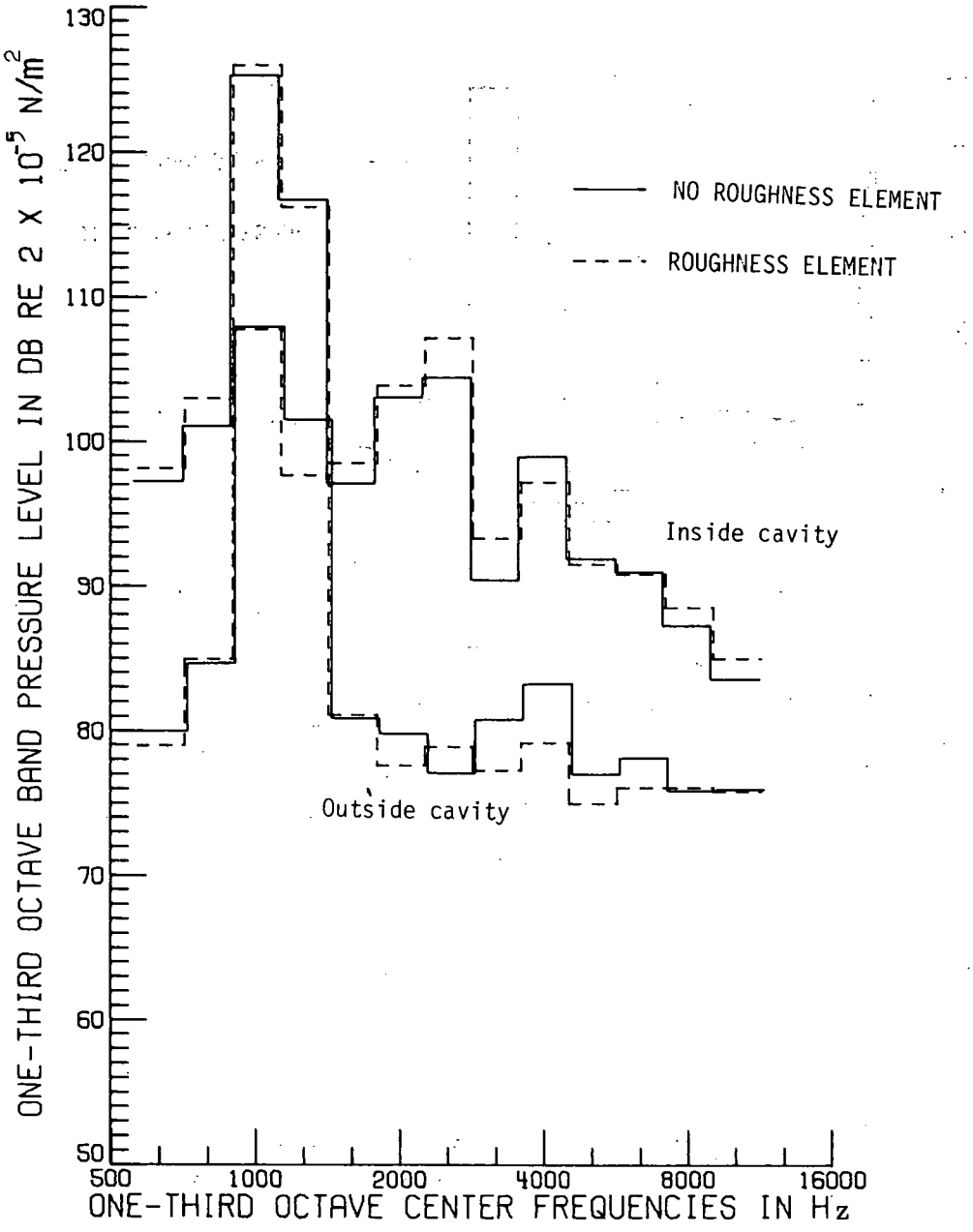

(e) Case 5. V = 86 m/sec; L/D = 1.4.

Figure 6.- Continued.

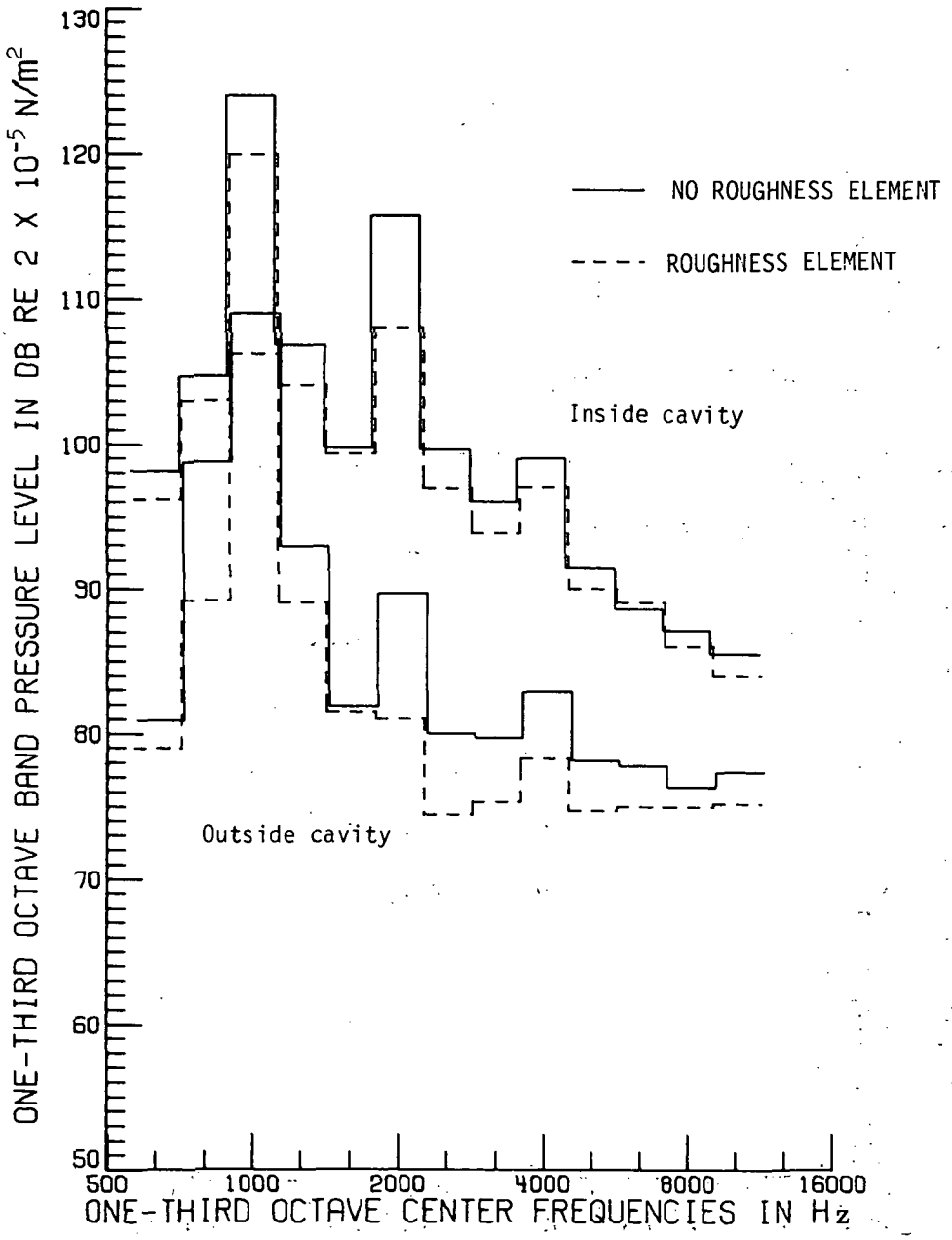

(f) Case 6. V = 86 m/sec; L/D = 1.6.

Figure 6.- Continued.

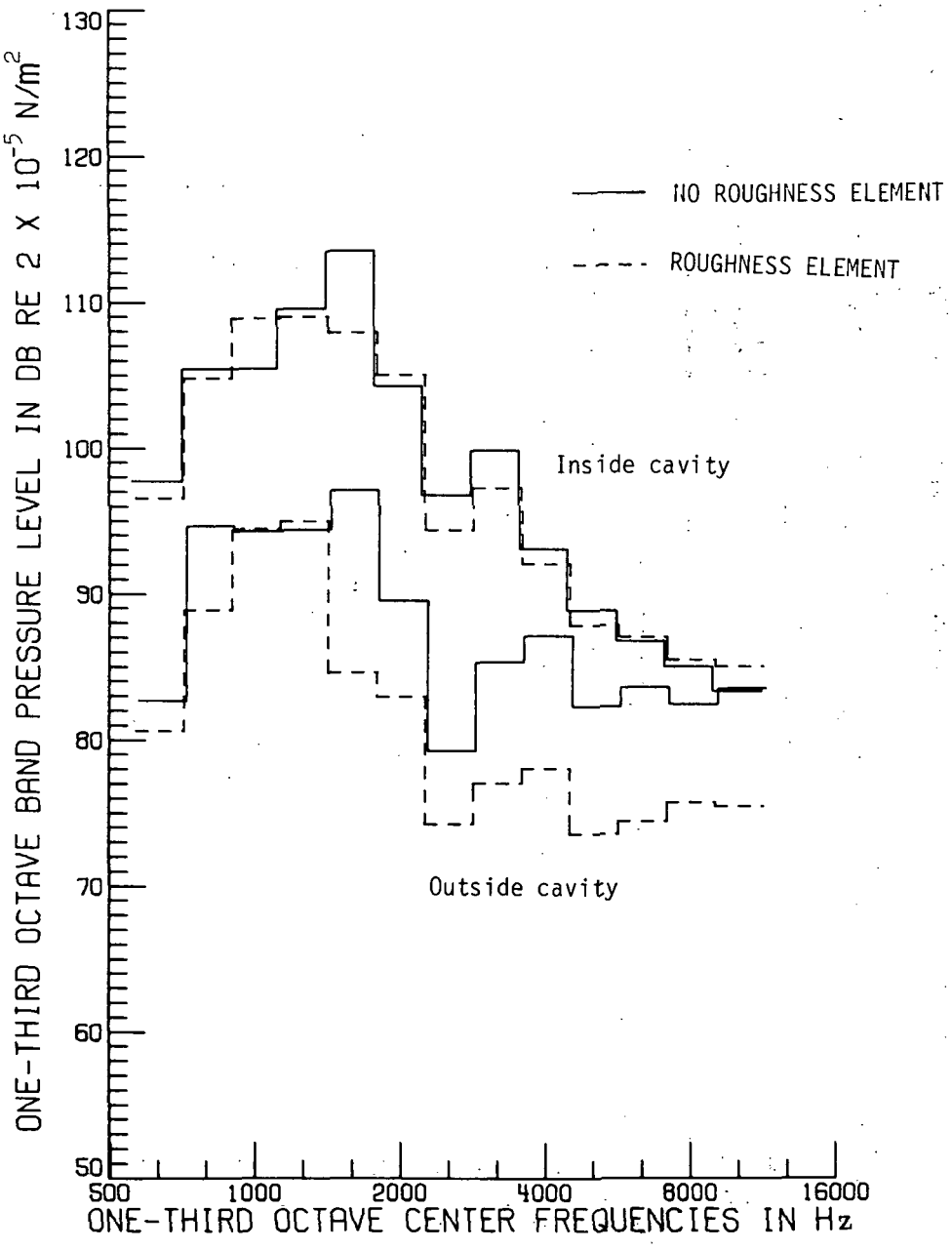

(g) Case 7. V = 86 m/sec; L/D = 2.

Figure 6.- Continued.

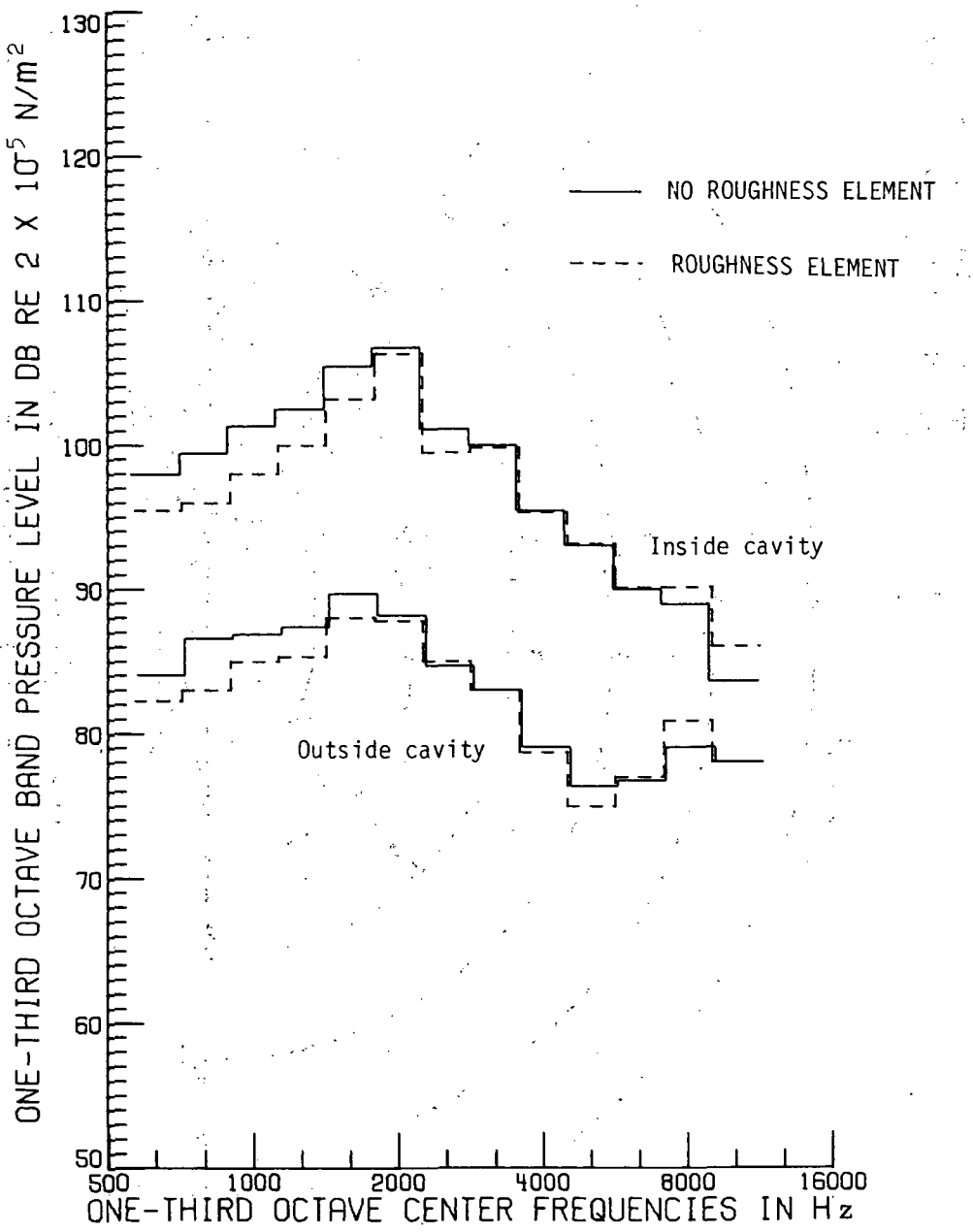

(h) Case 8. V = 86 m/sec; L/D = 4.

Figure 6.- Concluded.

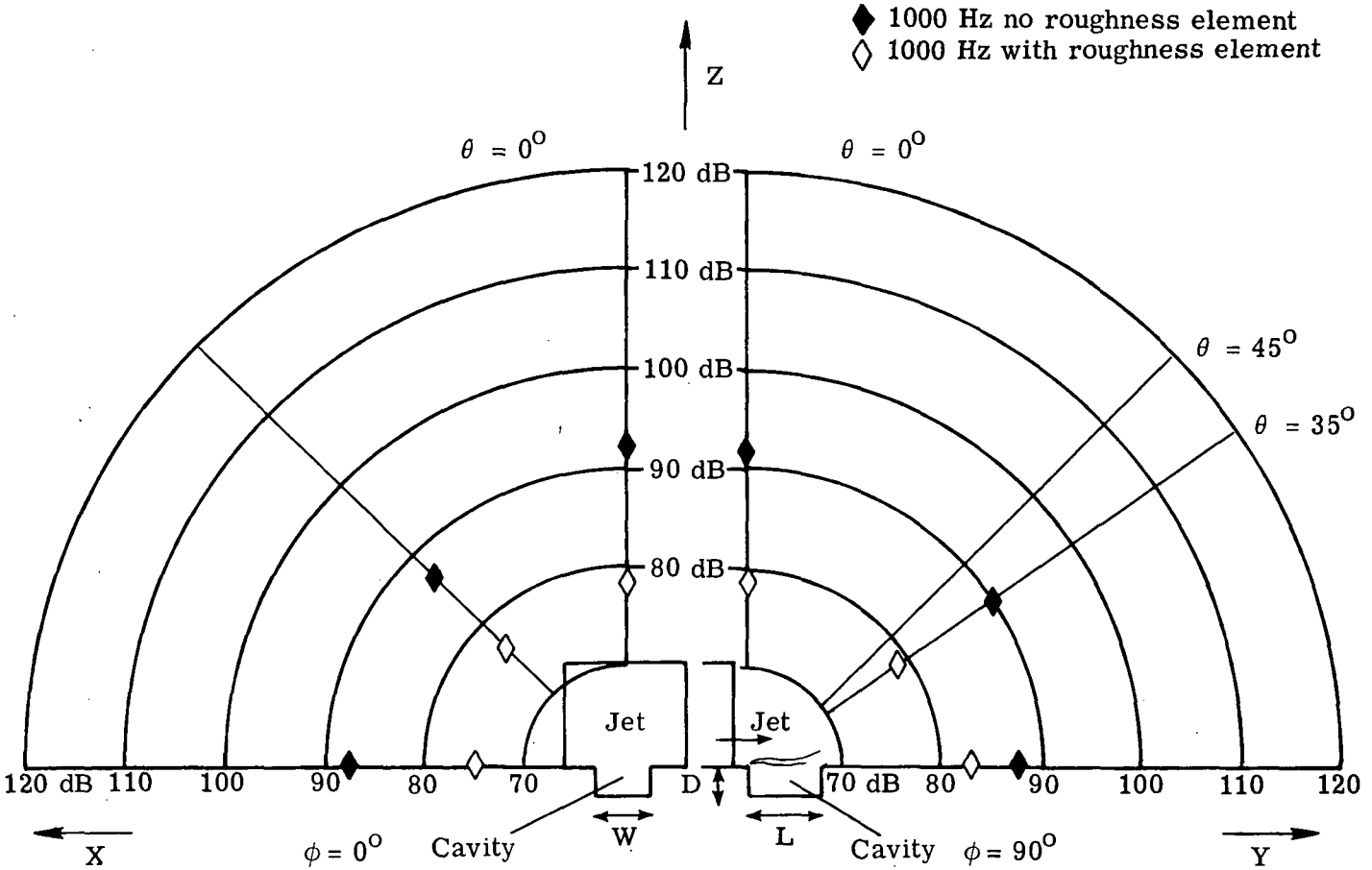

(a) Case 1. V = 43 m/sec; L/D = 1.

Figure 7.- Directivity patterns.

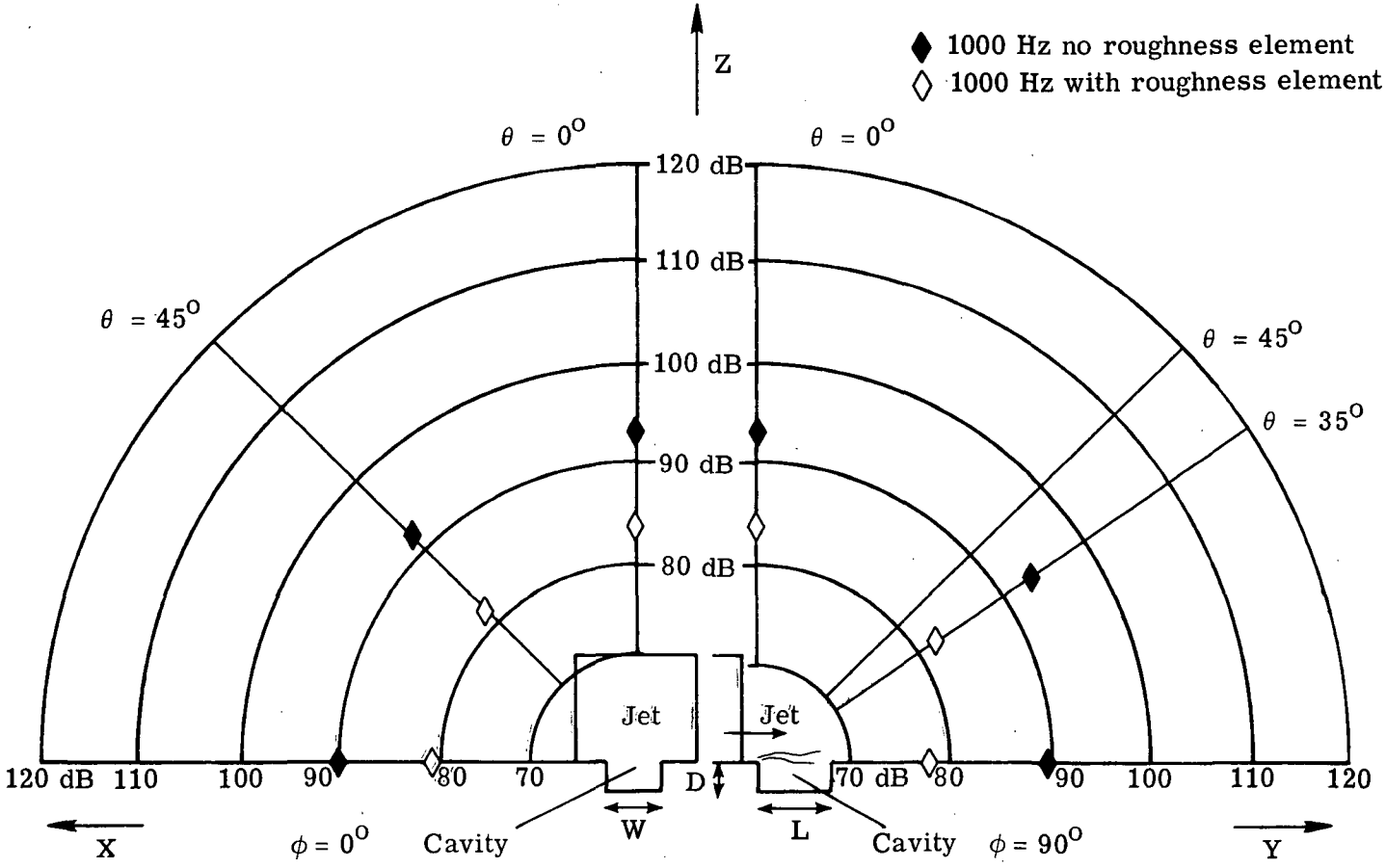

(b) Case 2. V = 43 m/sec; L/D = 1.4.

Figure 7.- Continued.

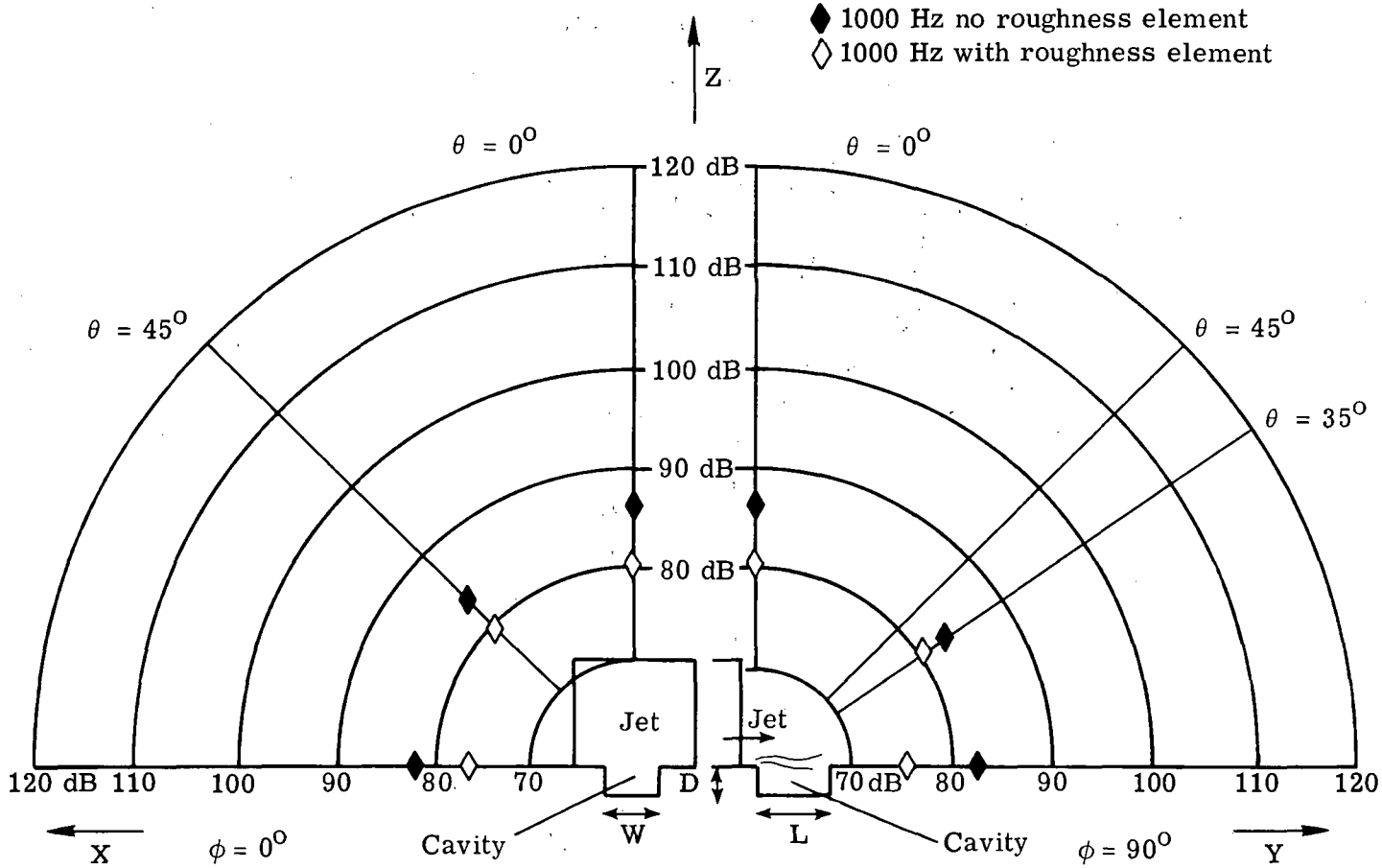

(c) Case 3. V = 43 m/sec; L/D = 1.6.

Figure 7.- Continued.

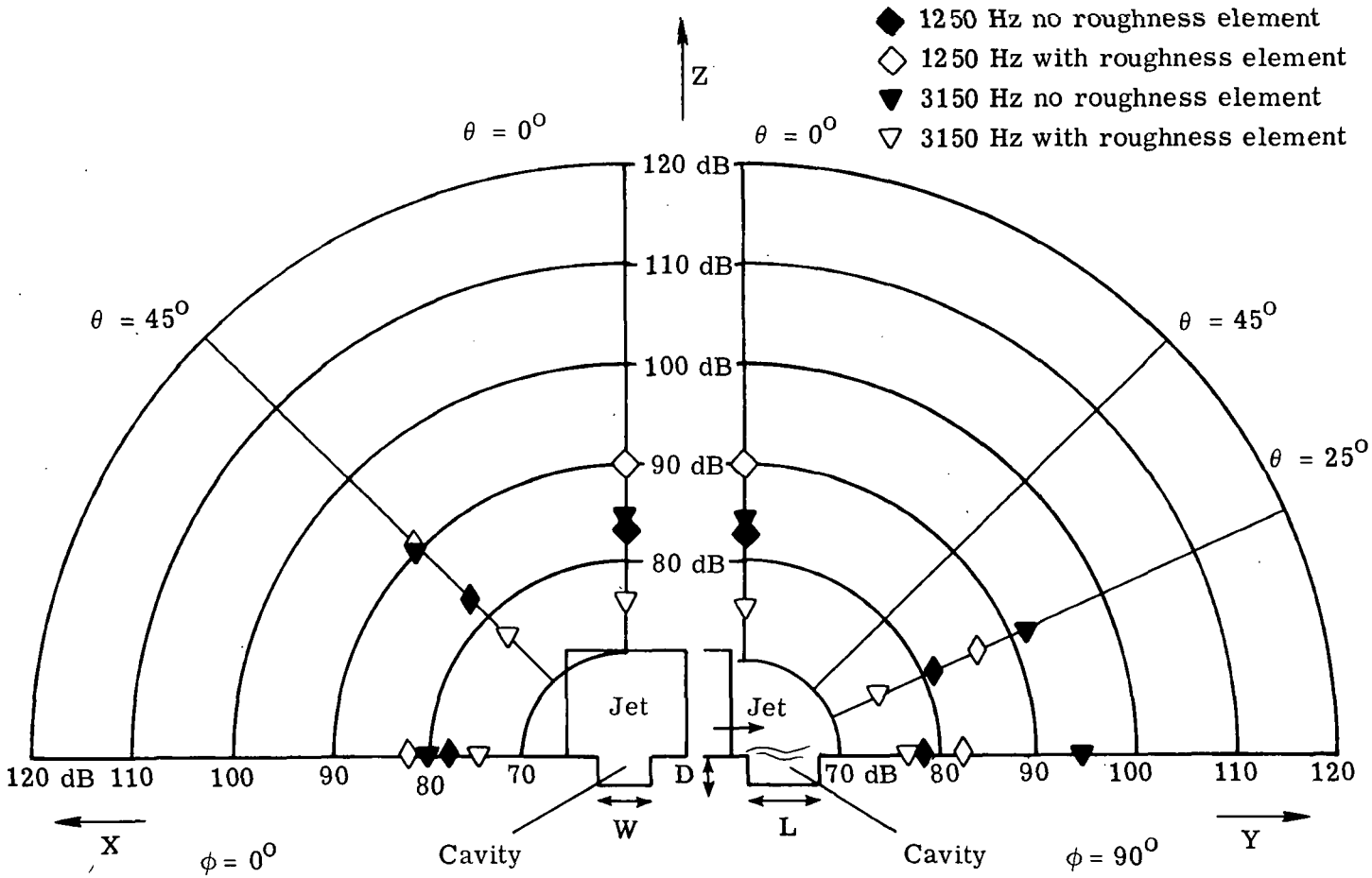

(d) Case 4. V = 86 m/sec; L/D = 1.

Figure 7.- Continued.

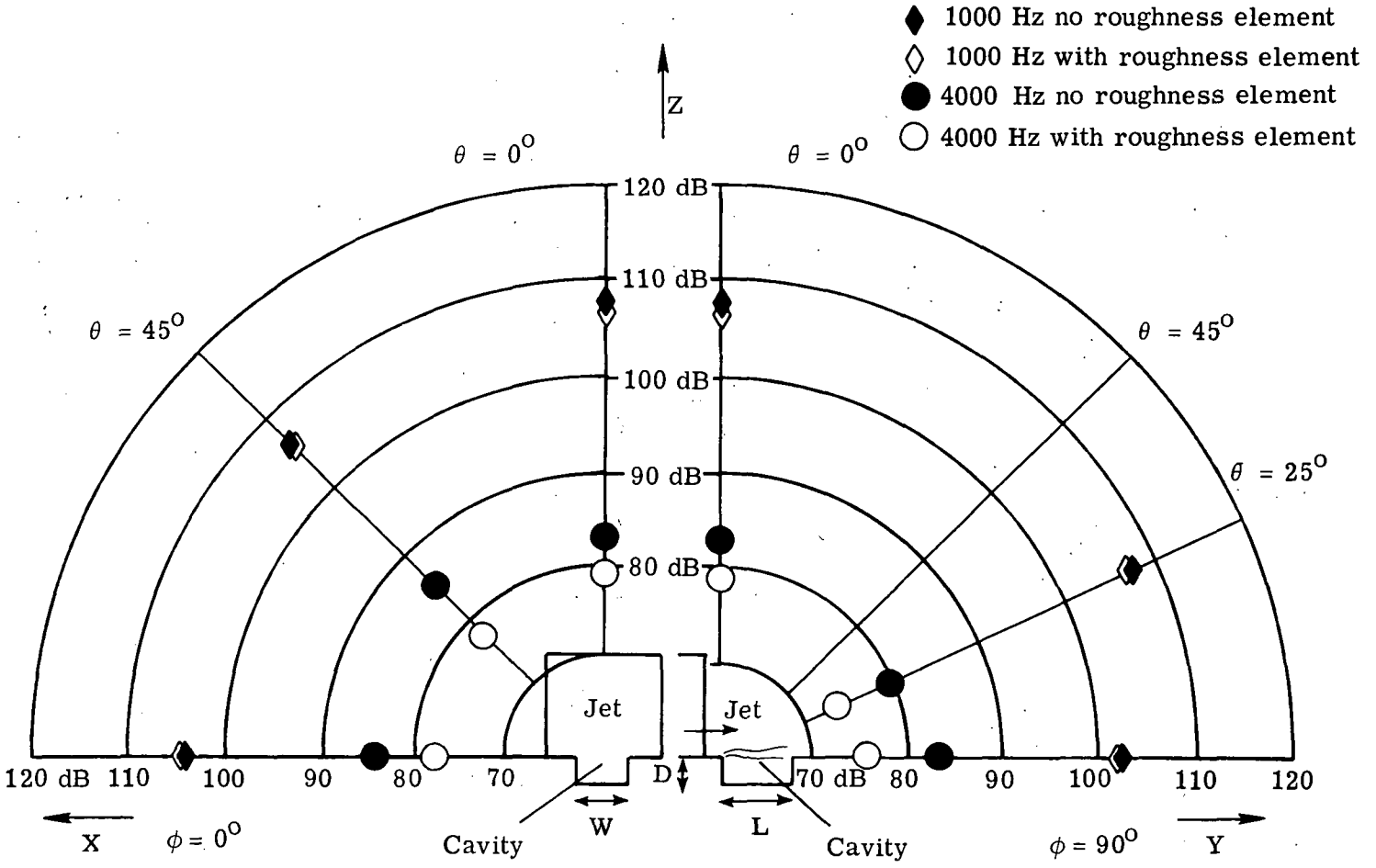

(e) Case 5. V = 86 m/sec; L/D = 1.4.

Figure 7.- Continued.

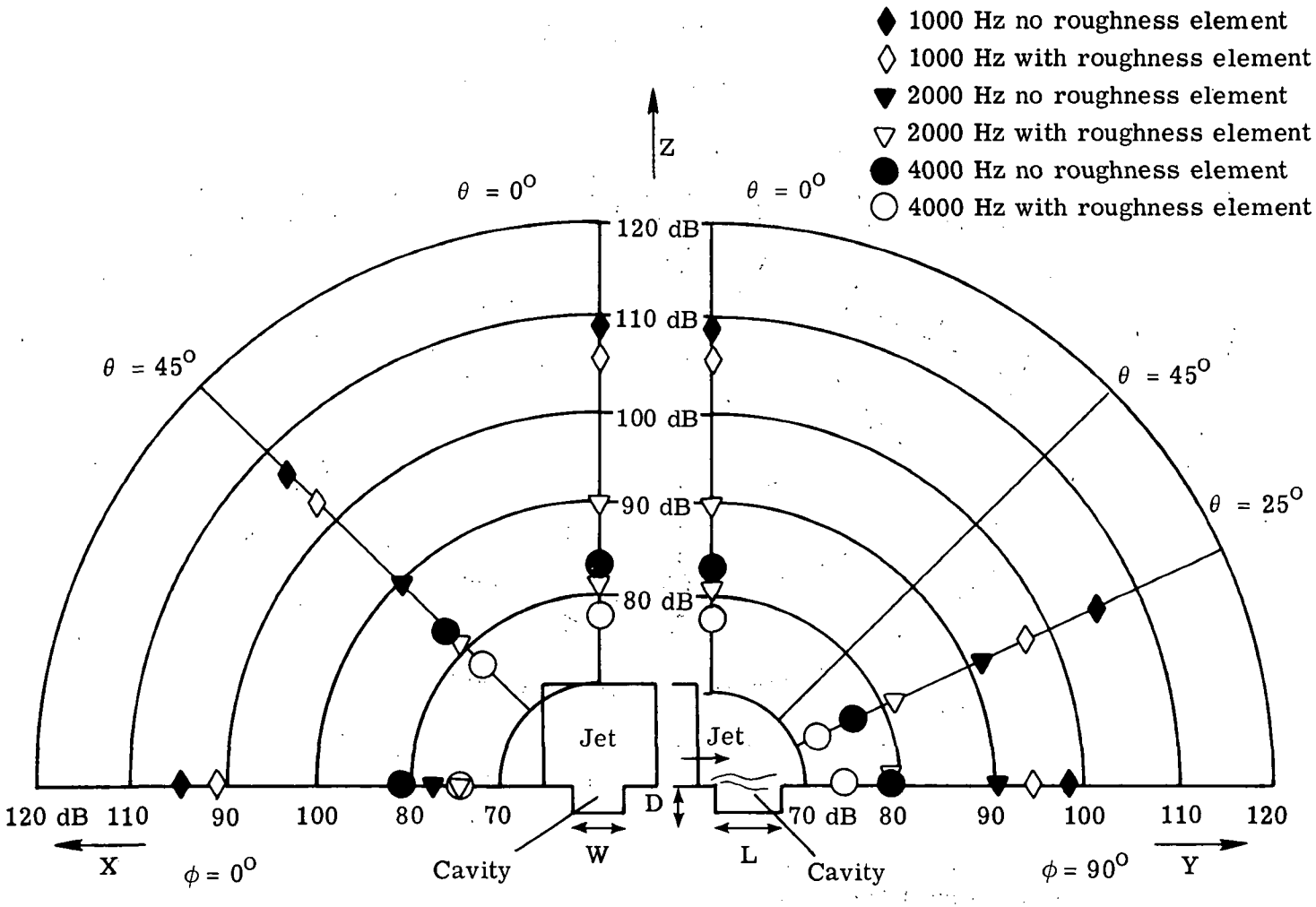

(f) Case 6. V = 86 m/sec; L/D = 1.6.

Figure 7.- Continued.

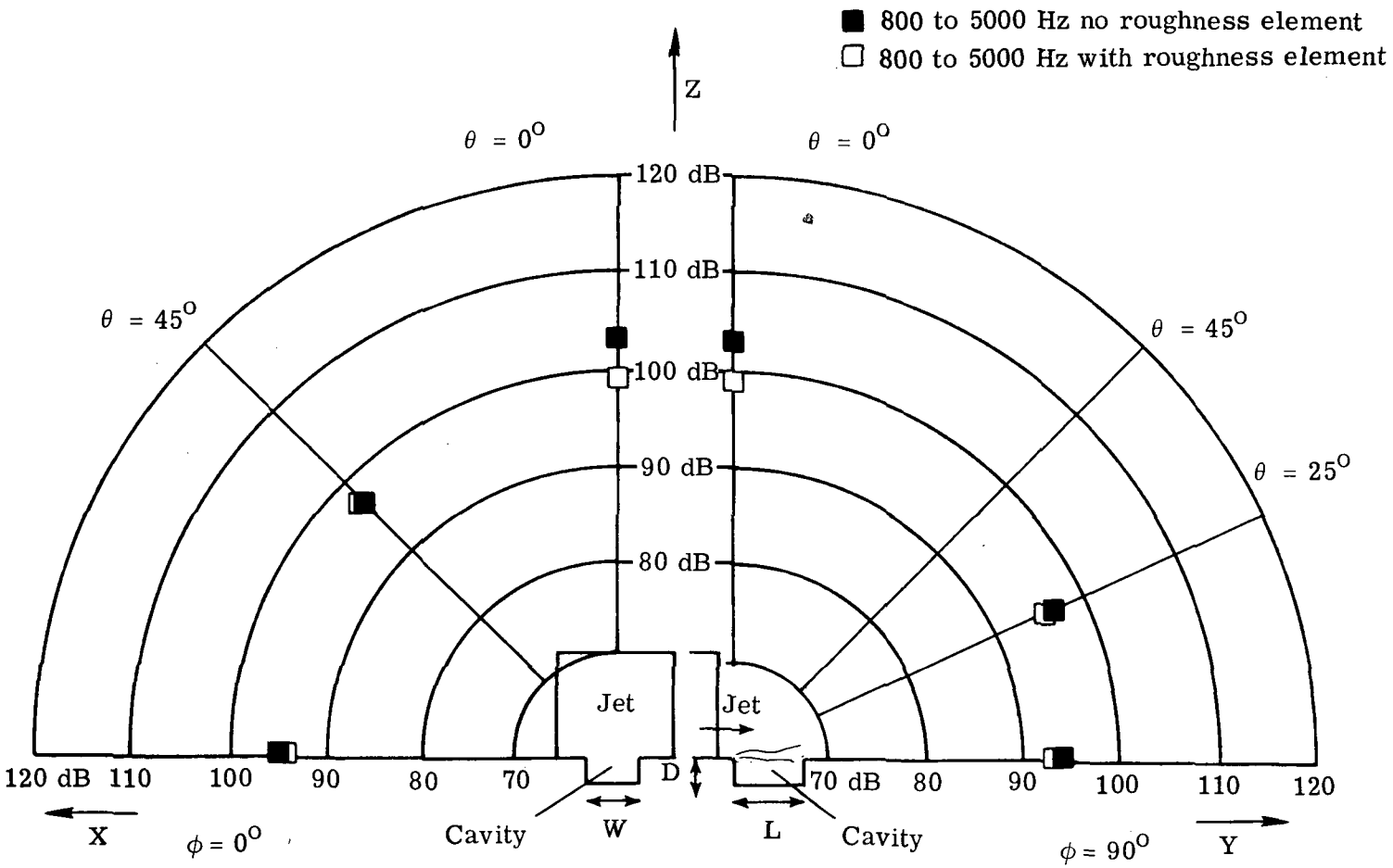

(g) Case 7. V = 86 m/sec; L/D = 2.

Figure 7.- Continued.

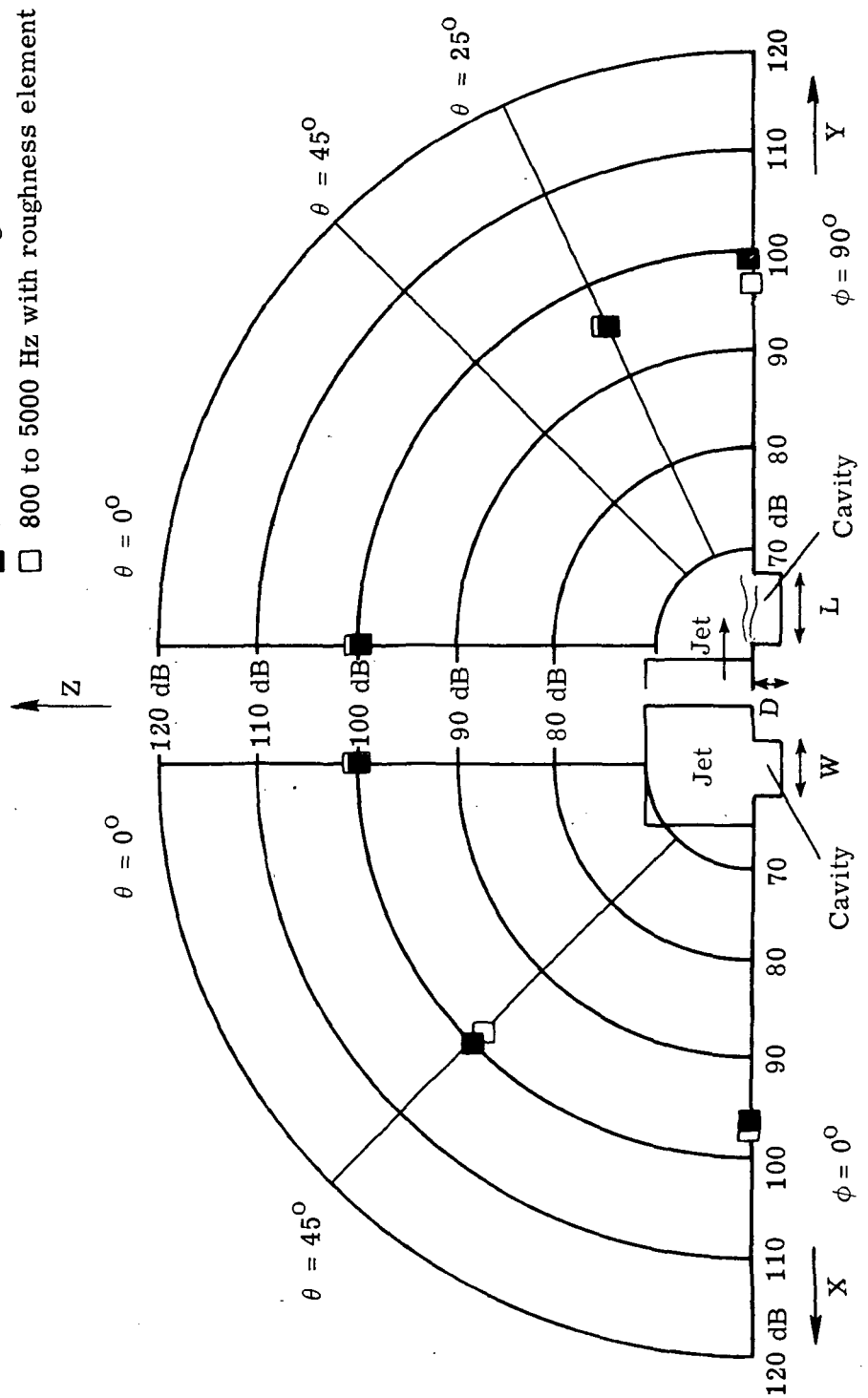

(h) Case 8. V = 86 m/sec; L/D = 4.

Figure 7.- Concluded.

NATIONAL AERONAUTICS AND SPACE ADMINISTRATION
WASHINGTON, D.C. 20546

OFFICIAL BUSINESS
PENALTY FOR PRIVATE USE $300

SPECIAL FOURTH-CLASS RATE
BOOK

POSTAGE AND FEES PAID
NATIONAL AERONAUTICS AND
SPACE ADMINISTRATION
451

U.S.MAIL

POSTMASTER : If Undeliverable (Section 158 Postal Manual) Do Not Return

"The aeronautical and space activities of the United States shall be conducted so as to contribute . . . to the expansion of human knowledge of phenomena in the atmosphere and space. The Administration shall provide for the widest practicable and appropriate dissemination of information concerning its activities and the results thereof."

—NATIONAL AERONAUTICS AND SPACE ACT OF 1958

NASA SCIENTIFIC AND TECHNICAL PUBLICATIONS

TECHNICAL REPORTS: Scientific and technical information considered important, complete, and a lasting contribution to existing knowledge.

TECHNICAL NOTES: Information less broad in scope but nevertheless of importance as a contribution to existing knowledge.

TECHNICAL MEMORANDUMS: Information receiving limited distribution because of preliminary data, security classification, or other reasons. Also includes conference proceedings with either limited or unlimited distribution.

CONTRACTOR REPORTS: Scientific and technical information generated under a NASA contract or grant and considered an important contribution to existing knowledge.

TECHNICAL TRANSLATIONS: Information published in a foreign language considered to merit NASA distribution in English.

SPECIAL PUBLICATIONS: Information derived from or of value to NASA activities. Publications include final reports of major projects, monographs, data compilations, handbooks, sourcebooks, and special bibliographies.

TECHNOLOGY UTILIZATION PUBLICATIONS: Information on technology used by NASA that may be of particular interest in commercial and other non-aerospace applications. Publications include Tech Briefs, Technology Utilization Reports and Technology Surveys.

Details on the availability of these publications may be obtained from:

SCIENTIFIC AND TECHNICAL INFORMATION OFFICE

NATIONAL AERONAUTICS AND SPACE ADMINISTRATION

Washington, D.C. 20546